People's Democratic Republic of Algeria
Ministry of Higher Education and Scientific Research
University Mohamed Boudiaf - M'sila

Faculty: Technology
Domain: Sciences and Technologies
Department: Electronics
Field: Telecommunications
Specialty: Telecommunications Systems

Thesis submitted for the award of

the Academic Master's degree

Presented by: Mohamed DJABALLAH

Title

Analysis of Smallest-Of Cell Averaging CFAR Detection in Homogeneous Gamma-Distributed Background

Defended before the jury composed of:

Dr. Ali KHALFA	University of M'sila	Examiner
Dr. Mohamed SAHED	University of M'sila	Supervisor
Dr. Abdelghafour HERIZI	University of M'sila	Examiner

Academic year: 2024 / 2025

Acknowledgments

I would like to express my deepest gratitude and sincere appreciation to my supervising professor, **Dr. SAHED Mohamed** for his supervision and support during the completion of my master's thesis in communication systems for their invaluable guidance, unwavering support, and constructive feedback throughout the course of this research Your expertise, patience, and encouragement have played a crucial role in shaping this thesis and in enriching my academic journey. Thank you for believing in my potential and for generously sharing your time and knowledge. It has been an honor to learn under your supervision. Our thanks also to Dr. Ali KHALFA and Dr. Abdelghafour HERIZI for accepting to judge our work Our gratitude also goes to the head of the electronics department, **Dr. M. TABBAKH**, for his unwavering support and encouragement. We are also grateful to all the teachers of the specialty telecommunication systems for each with its name for their enriching teachings. Additionally, we would like to acknowledge for our colleagues for their companionship and mutual support. Finally, our heartfelt appreciation is directed to everyone who played a role in this endeavor, contributing both directly and indirectly to my success.

Dedication

I dedicate this thesis to my beloved parents, whose unwavering support, encouragement, and sacrifices have made this journey possible.

To all my sisters, for their companionship and belief in me.

To my friends: Moussa Boucherit, Abdnour Helalli, ayoub Berrabah, safwane Fadel, Islam Ferhat , Yacine Tayab, for their camaraderie and good cheer.

And to all those who have contributed, from near or far, to this achievement your part in my journey will always be cherished I am deeply thankful for all whose contribution to my success.

Mohamed DJABALLAH

Contents

List of Figures

List of Tables

General Introduction

Several non-Gaussian statistical models have been proposed in the literature to characterize the random behavior of modern radar clutter. These models include the Log-normal, Weibull, Positive Alpha-Stable, Pareto, and K distributions [1–3]. They have been extensively employed in the analysis and design of constant false alarm rate (CFAR) detection schemes [1–6].

It is well established that, regardless of the selected clutter model, the performance of a CFAR detector is primarily governed by two key metrics: the probability of detection (P_d) and the probability of false alarm (P_{fa}). However, the derivation of closed-form expressions for these metrics is often hindered by the mathematical complexity introduced by non-Gaussian clutter models. This challenge underscores the importance of identifying non-Gaussian distributions that not only accurately describe the clutter but also permit the derivation of tractable, preferably closed-form, analytical expressions for P_d and P_{fa}.

Recent studies have demonstrated that the Gamma distribution provides an accurate statistical representation of high-resolution clutter data obtained from X-band maritime radar operating at low-grazing angles [11]. Moreover, performance analyses of various CFAR detectors under the assumption of Gamma-distributed clutter have been investigated in [7, 11]. For example, Zhou et al. introduced the CA-CFAR, GO-CFAR, and SO-CFAR detection schemes under the assumption of a homogeneous background scenario [11]. A key contribution of their work was the derivation of the corresponding P_{fa} expressions for the considered detectors. Unfortunately, these expressions were presented in the form of integrals, as shown in Eqs. (19) and (22) of [11], which the authors claimed could not be expressed in closed form but could be evaluated numerically.

In the present study, motivated by the need for more practical and analytically tractable CFAR detection schemes, we demonstrate that the aforementioned integrals can, in fact, be reduced to exact closed-form expressions. Specifically, we derive explicit expressions for the P_{fa} of the CA-, GO-, and SO-CFAR detectors in terms of the Gauss hypergeometric function and the second Appell function, respectively. To the best of our knowledge, this represents the first instance in the literature where such closed-form expressions have been obtained for these detectors. Additionally,

we introduce original approximations for the probability of detection (P_d) for both schemes, further contributing to the analytical tractability and practical implementation of CFAR detectors. This constitutes the main contribution of this dissertation

Chapter I: Fundamentals of Signal Detection in Noise

I.1 Introduction

The field of signal detection and parameter estimation focuses on analyzing received signals to determine whether signals of interest are present , classify detected signals , and extract information—either intentionally embedded or inadvertently included. Detecting signals in noisy environments is a fundamental challenge in signal processing, requiring the extraction of weak signals from background noise. This task is particularly difficult because noise can obscure signals, making them harder to distinguish.

This problem is critical in applications such as radar, sonar, communications, and medical imaging, where signals are often buried in noise from various sources. For instance, in active radar, electromagnetic pulses or pulse trains are transmitted, and the reflected signals are analyzed to identify air traffic , determine distance and speed, and potentially generate images for aircraft classification. Similarly, in sonar signal processing, active sonar systems send sound pulses into the ocean and analyze return echoes using methods akin to those used in radar.

A range of techniques from simple threshold-based methods to advanced statistical and machine learning approaches are employed for signal detection. Ongoing advancements in this field have the potential to drive new capabilities in areas such as remote sensing[01].

I.2 Decision Theory

Decision theory is widely applied in fields such as radar, sonar, digital communication, and ultrasonic imaging to differentiate between signals carrying meaningful information and those affected by noise or interference. In a binary detection scenario within a digital communication system, a sequence of zeros and ones is transmitted through a medium. As the signals travel, they become distorted by additive noise from the medium as well as noise introduced by the receiver. Since the receiver cannot inherently distinguish whether a received signal corresponds to a zero or a one, it must apply a decision-making process to determine the most likely interpretation. This decision-making process falls under the theory of signal detection. This scenario can be modeled as a source emitting one of two possible outputs at different points in time. These outputs, referred to as hypotheses, define the detection framework: the null hypothesis (H_0) represents a zero

(indicating the absence of a target), while the alternative hypothesis (H_1) represents a one (indicating the presence of a target). as shown in Figure [02]:

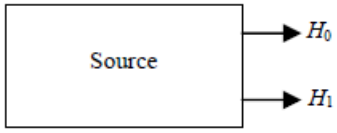

Figure I.1: Source for binary hypothesis

If Y falls within Z_0, the receiver selects H_0, whereas if Y falls within Z_1 , the receiver opts for H_1, as illustrated in Figure I.2 . The observation space Z is the combination of Z_0 and Z_1, expressed as: $Z= Z_0 \cup Z_1$

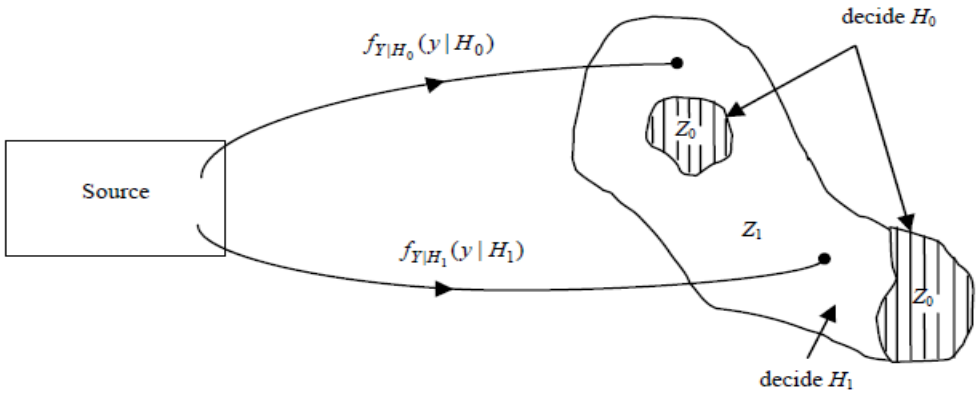

Figure I.2:: Decision regions

The probability density functions of Y corresponding to each hypothesis are $f_{y|H_0}(y|H_0)$ and $f_{y|H_0}(y|H_1)$, where y is a particular value of the random variable Y.

Classical detection theory assumes prior knowledge of the probability distribution functions for both hypotheses. The detector design can be derived using the Bayes likelihood ratio based on these distributions. Given the prior density functions of the random variable X and an observed value $\varkappa$, the optimal detector is defined by the likelihood ratio $L(\varkappa)$ [03] [04]:

$$L(x) = \frac{f_x(x|H_1)}{f_x(x|H_0)} \tag{1.1}$$

The statement explains that there are two conditional probability densities, P(X|H_1) and P(X|H_0), which describe the probability of an event X given two different conditions, H_1 and H_0. A decision is then made by comparing a test statistic, T(X), to a threshold value, λ. This threshold value is chosen based on the expected performance of the detector.

$$L(x)=\begin{cases} >^{\lambda\ accpt\ H_1} \\ \leq_{\lambda\ accpt\ H_0} \end{cases} \tag{1.2}$$

The statement explains that if an equality condition is met, a random decision-making rule can be applied. This rule typically assigns equal probability to selecting between two hypotheses but may be adjusted based on the detector's performance criteria or the associated cost of each hypothesis. Currently, the equality condition is set for H_0 to reduce the likelihood of incorrectly accepting H_1, which is a critical consideration discussed further later.

The effectiveness of a detector in identifying errors depends on the threshold set to either control the probability of a false alarm or the probability of a miss. Typically, a false alarm is more concerning than a miss, as accepting hypothesis H_1 incorrectly can have serious consequences.

Therefore, selecting an optimal threshold λ for the detector requires considering constraints on the probability of false alarms. The probability of a false alarm, P_{fa}, can be determined using the Neyman-Pearson criterion. This criterion formulates the hypothesis testing problem as a constrained optimization problem, where the probability of detection is maximized while ensuring the false alarm probability remains within an upper bound [04]:

$$P_{fa} = \int_{\lambda}^{\infty} P\big(L(x|H_0)\big)dL(x) \leq \alpha \qquad for\ all\ x \tag{1.3}$$

The size of the detector, denoted as quantity α, is a fixed parameter. This ensures that, regardless of the observations X , the probability of a false alarm will not exceed a predetermined level. This concept is known as Constant False Alarm Rate (CFAR) analysis, which serves as an optimization constraint in various detectors discussed in this thesis.It is important to note that the threshold for target detection is not based on any prior information about the target itself. As a result, the detector's probability of successfully detecting the target may vary depending on the target's distribution.

Let's focus on the problem of testing a simple null hypothesis, H_0, against a simple alternative hypothesis, H_1. We denote this by: $\beta = P_{H_0}[accept\ H_0]$

The probability of a Type II error refers to accepting the null hypothesis H_0 when, in reality, the alternative hypothesis H_1 is true. In this context, $P_{H_1}[E]$ represents the probability of an event E given that H_1 is true. Equivalently: $1-\beta = P_{H_1}[rejectH_0]$

Although the likelihood of committing a Type I error is guaranteed to be below a specified level α\alphaα for all observations under the null hypothesis H_0, the occurrence of a Type II error depends on the statistics of the alternative hypothesis H_1.

To calculate the probability of a missed detection (Type II error), denoted as P_m, one must evaluate the integral of the test statistic presented in equation (1.4) [03].

$$P_m = \int_{-\infty}^{\lambda} P\big(L(x|H_0)\big)dL(x) = 1 - \beta \tag{1.4}$$

The probability of missing a target is represented as $1-\beta$, while the probability of detecting it, denoted as P_d , represents the likelihood of correctly identifying the target. The probability of detection depends on the threshold λ , which is predetermined based on the statistics of the null hypothesis and is selected to satisfy the CFAR constraint.This implies that the detector's performance, in terms of detection probability, cannot be improved for a fixed false alarm rate α , regardless of the target statistics [05] [06] [07].

I.3. Statistical clutter models

Statistical clutter models are widely used in various fields, particularly in radar and communications, to describe interference or unwanted signals that complicate the detection and interpretation of desired signals. In statistical terms, clutter is often modeled as a random process that affects the detection and estimation performance of systems such as radar, sonar, and wireless communications. These models help predict how clutter behaves under different conditions, enabling the development of better detection algorithms and improved signal processing techniques.This section introduces the different statistical models of sea clutter found in the literature and provides an in-depth discussion of the properties that explain the random nature of radar clutter. However, to maintain brevity, this dissertation will not cover the experimental validation of these statistical models. For further details on the experimental modeling and

validation of sea clutter, please refer to relevant literature.Table I.1 presents a summary of the main differences between noise and clutter returns. These two phenomena are modeled differently due to their unique characteristics, and it has been observed that they exhibit distinct properties [08].

Noise signal	Clutter signal
Amplitude is independent of the transmitted radar Signal	Amplitude is proportional to the transmitted signal
Wide bandwidth	Narrow bandwidth
Independent of environmental parameters	Can vary with changing environmental conditions

Table I.1: Clutter versus Noise

I.3.1. Gaussion clutter models

I.3.1.1. Normal distribution

The probability density function (PDF) describres the characteristics of the normal distribution also known as the Gaussion distribution . it is defined as follows:

$$f_x(x) = \frac{1}{\sigma\sqrt{2\pi}} \exp\left(-\frac{(x-\mu)^2}{2\sigma^2}\right) \quad (1.5)$$

Where μ $is\ the\ mean\ and\ \sigma^2\ is\ the\ variance\ of\ X.the\ probability$ density function (PDF) of the normal distribution is represented in Figure 1.3

Using the definition of the error function (erf(x)) , the cumulative distribution function (CDF) can be given as follows[09]:

$$f_x(x) = \mathrm{P}(\mathrm{X} \leq \mathrm{x}) = \frac{1}{2}\left[1 + \mathrm{erf}\left(\frac{x-\mu}{\sigma\sqrt{2}}\right)\right] \quad (1.6)$$

It follow that :

$$\mathrm{erf}(z) = \frac{2}{\sqrt{\pi}} \int_0^z e^{-t^2}\, dt \quad (1.7)$$

This function is useful for finding probabilities in a normal distribution such as in hypothesis testing and confidence interval calculations.

The moments about the mean of this distribution are :

$$E[x^n] = \begin{cases} 0 & f\ or\ odd \\ \frac{n!\sigma^n}{\left\{\frac{n}{2}\right\}!2^{\frac{n}{2}}} & f\ or\ even \end{cases} \quad (1.8)$$

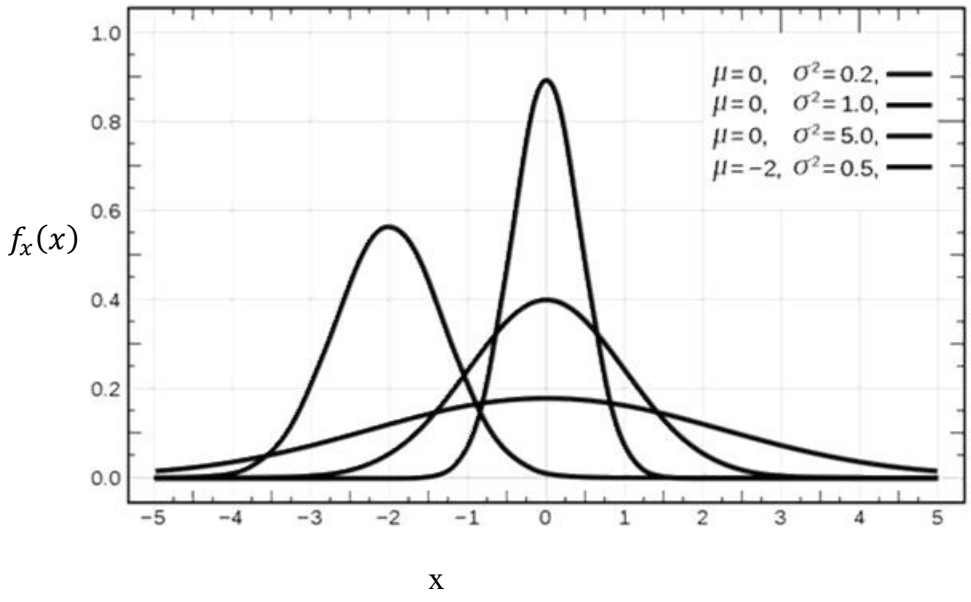

Figure I.3: probability density function of the Gaussion distribution

I.3.1.2. Rayleigh distution

the Rayleigh Distution ,a type of Gaussian model , is a continuous probability distribution commonly used in signal processing , radar and wireless communication. It is often applied to model fading signals and noise amplitude, as depicted in Figure 1.4:

$$f_x(x) = \frac{x}{b^2}\exp\left(-\frac{x^2}{2b^2}\right), \quad x \geq 0, \qquad \sigma > 0 \quad (1.9)$$

Where b is the scale parameter, which determines the spread of the distribution .

and the corresponding cumulative distribution function is given by:

$$f_x(x) = 1 - \exp\left(-\frac{x^2}{2\sigma^2}\right), \quad x \geq 0, \quad (1.10)$$

Where b is the scale parameter of the Rayleigh Distution.

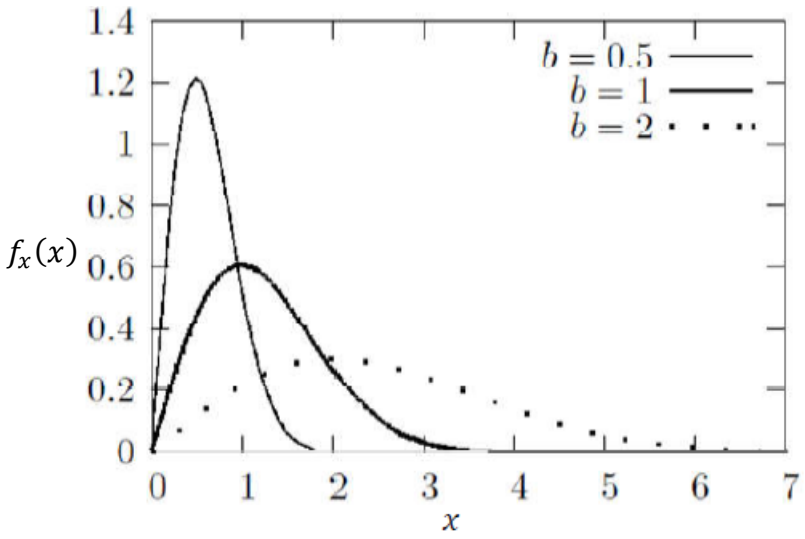

Figure I.4: Probability density function of the Rayleigh distribution

I.3.2. Non-gaussian clutter models

I.3.2.1. Lognormal distribution

A Lognormal Distribution is a continuous probability distribution of a random variable whose logarithm is normally distributed. In other words. If X is lognormally distributed , then Y=$ln(X)$ follows a normal distribution [10]:

$$f_x(x) = \begin{cases} \frac{1}{\sqrt{2\pi}x\sigma} \exp\left(-\frac{(\ln(x)-\mu)^2}{2\sigma^2}\right), x \geq 0 \\ 0\ ; \qquad\qquad otherwise \end{cases} \tag{1.11}$$

Where μ is the mean and $2\sigma^2$ is the variance of the lognormal distribution. The corresponding CDF can be expressed simply in terms of the error function, as follows:

$$f_x(x) = \mathrm{P}(\mathrm{X} \leq \mathrm{x}) = \frac{1}{2}\left[1 + \mathrm{erf}\left(\frac{\ln(x)-\mu}{\sigma\sqrt{2}}\right)\right] \tag{1.12}$$

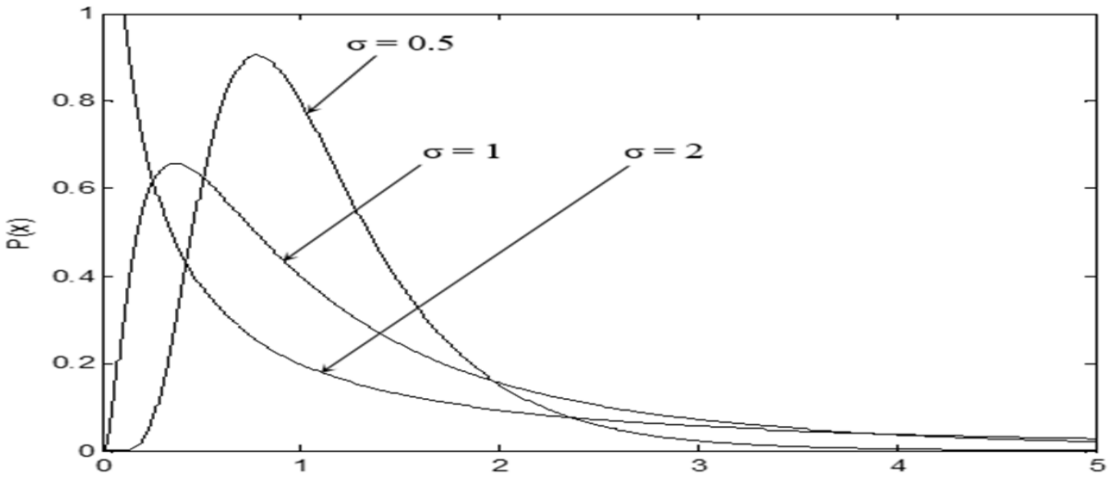

Figure I.5: Probability density function of the lognormal distribution

I.3.2.2 Weibull-distribution model

The Weibull distribution is a continuous probability distribution widely used in reliability analysis, survival analysis, and failure modeling. It is defined by two or three parameters, as shown in Figure 1.6. Its probability density function is given by:

$$f_x(x) = \begin{cases} \frac{k}{\lambda}\left(\frac{x}{\lambda}\right)^{k-1} \exp\left(-\frac{x}{\lambda}\right)^{k}, x \geq 0 & k, \lambda > 0 \\ 0\,; & otherwise \end{cases} \quad (1.13)$$

Where k and λ are the shape and scale parameters of the Weibull-Distribution ,respectively. The corresponding coumulative distribution function (CDF) is given by :

$$f_x(x) = 1 - \exp\left(-\frac{x}{\lambda}\right)^{k} \quad (1.14)$$

The *n*-th moments of the Weibull distribution can be given by:

$$m_n = \lambda^n \Gamma\left(\frac{n}{k} + 1\right) \quad (1.15)$$

and consequently, the mean and variance of this distribution are, respectively:

$$E(x) = \lambda \Gamma\left(\frac{n}{k} + 1\right) \quad (1.16)$$

$$var(x) = \lambda^2 \left[\Gamma\left(\frac{2}{k} + 1\right) - \Gamma^2\left(\frac{1}{k} + 1\right)\right] \quad (1.17)$$

where Γ(·) denotes the Gamma function:

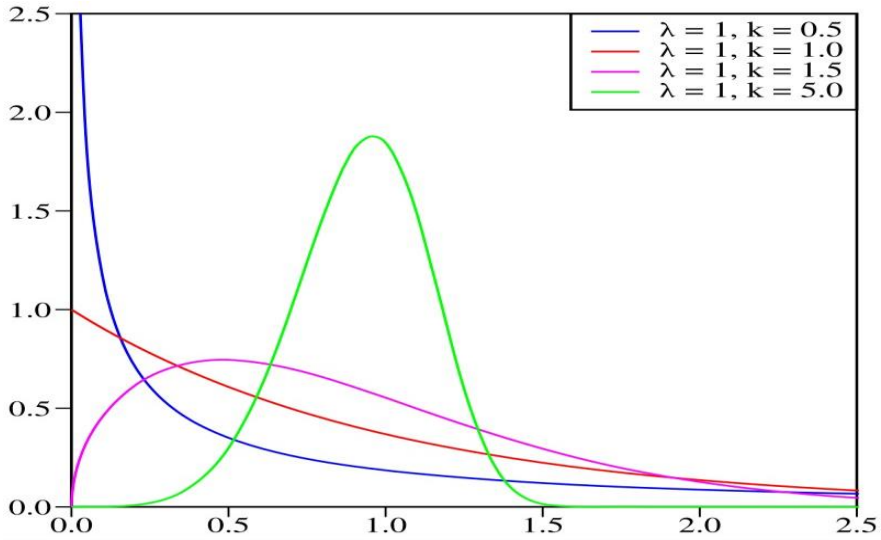

Figure I.6: Probability density function of the Weibull-distribution

I.3.2.3. K-distribution

K-Distribution is a concept used in atmospheric sciences and radiative transfer to efficiently approximate gas absorption spectra. The primary purpose of the K-distribution is to depict radar sea clutter[11].

$$f_x(x) = \begin{cases} \frac{4}{\lambda\Gamma(v)}\left(\frac{x}{\lambda}\right)^{v} k_{v-1}, & x \geq 0 \\ 0\ ; & otherwise \end{cases} \tag{1.18}$$

Where α and β are the shape and the scale parameters of the Gamma-distribution respectively, and $\Gamma(\alpha)$ denotes the Gamma function

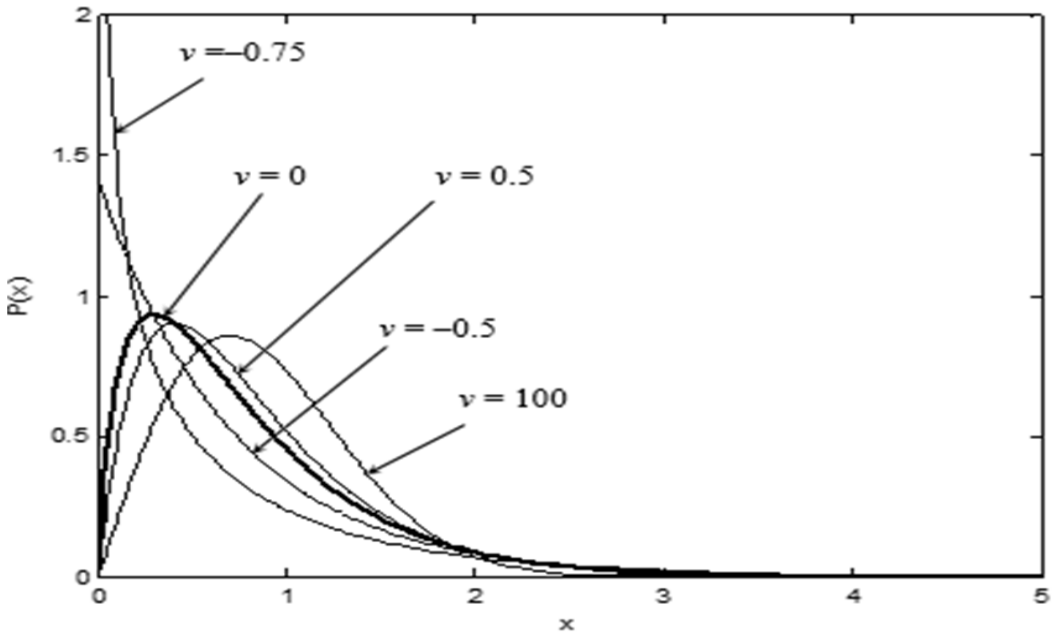

Figure I.7: Probability density function of the *K*-Distribution

I.3.2.4. Gamma-distribution

The Gamma distribution is a continuous probability distribution commonly used in statistics and probability theory. It is validated as a statistical model for high-resolution radar clutter. Its probability density function (pdf) is defined by:

$$f(x,k,\theta) = \frac{x^{k-1}e^{\frac{-x}{\theta}}}{\theta^k \Gamma(k)}, \qquad x > 0,\ k,\theta > 0 \tag{1.19}$$

$$\Gamma(k) = \int_0^\infty t^{k-1}e^{-t}\,dt \tag{1.20}$$

It follow that :

$$\mathrm{f}(\mathrm{x},\alpha,\beta) = \frac{\beta^{\alpha}\mathrm{x}^{\alpha-1}\mathrm{e}^{-\beta\alpha}}{\Gamma(\alpha)}, \qquad \mathrm{x} > 0,\ \alpha,\beta > 0 \tag{1.21}$$

Where α and β are the shape and the scale parameters of the Gamma-distribution respectively, and $\Gamma(\alpha)$ denotes the Gamma function

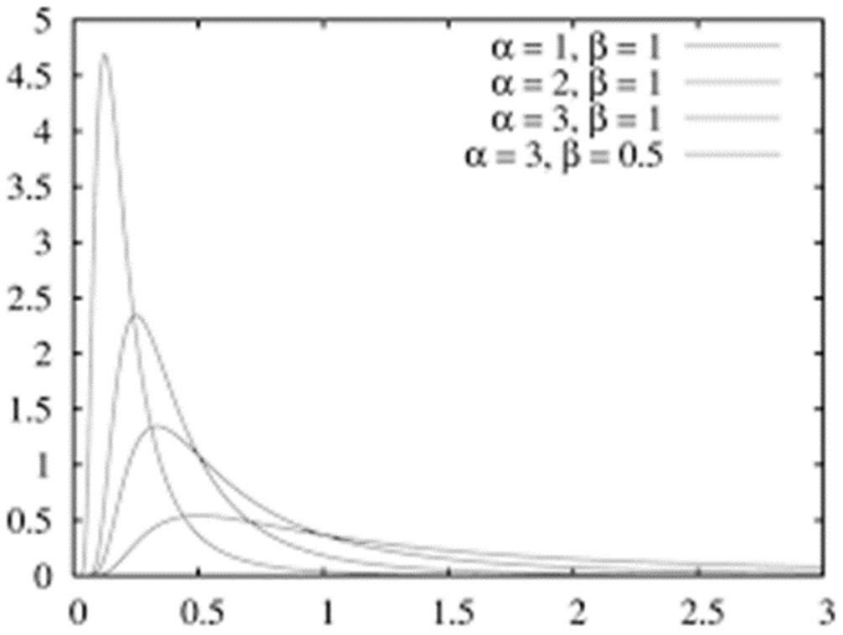

Figure I.8: Probability density function of the Gamma-distribution

I.4. Target signal models:

Target Signal Models refer to mathematical and statistical representations of signals received from a target in radar, sonar, communications, and other sensing applications. These models help characterize how a target reflects or emits signals and are crucial for detection, tracking, and classification. In this section, we will discuss models for different types of radar targets. This discussion is based on the concept of Radar Cross Sections (RCS) for simple point targets and extends to more complex cases involving targets with multiple scattering centers. In general, targets scatter energy in all directions. The RCS (σ) is a function of:

- Incident angle
- Scattering angle
- Signal frequency

Additionally, RCS depends on the shape of the target and the materials it is made of [18] [19].

Because the radar system and the target may be moving, the RCS value can change over time, causing targets to fluctuate. To simulate these fluctuations, four statistical models—referred

to as Swerling 1 through Swerling 4 are widely adopted in practice.The Swerling models categorize fluctuating targets based on:

- Two probability distributions
- Two time-varying behaviors

(See Table I.2 .)

Case	Probability Density Function	Fluctuation Period	Fluctuation Speed
Swerling I	Rayleigh	Dwell-to-Dwel	Slow fluctuating
Swerling II	Rayleigh	Pulse-to-Pulse	Fast fluctuating
Swerling III	Chi-square, degree 4	Dwell-to-Dwel	Slow fluctuating
Swerling IV	Chi-square, degree 4	Pulse-to-Pulse	Fast fluctuating

Table I.2: Swerling Target Models

I.4.1. Swerling I model

The Swerling I model is one of the most commonly used models in radar signal processing. It describes a fast-fluctuating target, where the Radar Cross Section (RCS) varies independently from pulse to pulse.This model is particularly useful for detecting:

- Aircraft
- Small objects
- Missiles

These targets scatter radar signals unpredictably. In the Swerling I model, the magnitude of the backscattered signal remains relatively constant during the dwell time. The RCS follows a Rayleigh distribution, given by[12]:

$$f_Y(y) = \frac{y}{\sigma_0^2} \exp\left(-\frac{y^2}{2\sigma_0^2}\right) \tag{1.22}$$

where $2\sigma_0^2$ is the arithmetic mean of all values of RCS of the reflecting object.

I.4.2. Swerling II model

The Swerling II model is a statistical model used in radar signal processing for slowly fluctuating targets. It is similar to the Swerling I model, as both use the same probability density function (PDF). However, in the Swerling II model, the radar cross-section (RCS) values change more rapidly, varying from pulse to pulse.

Both Swerling I and II models are applicable to targets consisting of multiple independent scatterers of roughly equal areas, such as airplanes. The key difference is that in the Swerling II case, instead of a rotating surveillance antenna, a target-tracking radar is used to focus on the target[12].

I.4.3. Swerling III model:

The Swerling III model describes fast-fluctuating targets where the Radar Cross Section (RCS) varies from pulse to pulse, similar to Swerling I. However, unlike Swerling I—which assumes a single dominant scatterer—Swerling III assumes multiple independent scatterers contributing to the RCS. The RCS fluctuation follows the distribution:

$$f_Y(y) = \frac{9y^3}{2\sigma_0^4} \exp\left(-\frac{3y^2}{2\sigma_0^2}\right) \tag{1.23}$$

I.4.4. Swerling IV model

The Swerling IV model is similar to the Swerling III model but describes a slowly fluctuating target with multiple independent scatterers. Unlike the Swerling III model, the radar cross-section (RCS) varies from pulse to pulse rather than from scan to scan. This characteristic makes it suitable for large aircraft, ships, and other stable targets with multiple reflective surfaces , and follows (1.23).

I.5. Radar detection principles

Previously, we observed that to apply Bayes' criterion, two assumptions are made:

1-The probability of occurrence of the two source outputs is known. These are the a priori probabilities, denoted as $P(H_0)$ and $P(H_1)$.

2-Since either hypothesis H_0or H_1 will always occur, their probabilities must sum to one: $P(H_0) + P(H_1) = 1$ Here, $P(H_0)$ represents the probability of hypothesis H_0 occurring, while $P(H_1)$ represents the probability of hypothesis H_1 occurring. For simplicity, we denote them as: P_0=$P(H_0)$, P_1=$P(H_1)$ Thus, we have: P_0+P_1=1

We have information about the a priori probabilities and cost assignments for all potential decisions. However, if we are unable to determine the a priori probabilities, the minimax criterion can be utilized. It is often challenging to assign realistic costs and a priori probabilities in certain physical scenarios, such as radar detection. To address this issue, we utilize the conditional probabilities of false alarm P_{fa} and detection P_d.

The Neyman-Pearson test mandates that we fix P_{fa} to a specific value α_0 while maximizing P_d. Since P_m = 1 - P_d, maximizing P_d is the same as minimizing P_m.

To ensure that $P_{fa} = \alpha_0$ and minimize P_m (maximize P_d), we utilize the calculus

of extrema and construct an objective function called J [13]:

$$J = P_m + \lambda(P_{fa} + \alpha_0) \tag{1.24}$$

Where $\lambda \geq 0$ is the lagrange multiplier.

It is important to note that there are various decision regions, Z_1 , within the observation space Z that satisfy the constraint $P_{fa} = \alpha_0$. The goal is to identify the decision regions that result in the minimum P_m. Therefore, we modify the objective function J to be expressed in terms of the decision region.

$$J = \int_{Z_1} f_y(y|H_1)\, dy + \lambda \left[\int_{Z_1} f_y(y|H_0)\, dy - \alpha_0\right] \tag{1.25}$$

As a result, the decision region Z_1 should be assigned values that satisfy $f_y(y|H_1) > f_y(y|H_0)$ to minimize the objective function J. Consequently, the decision rule can be defined as follows[14].

$$\frac{f_y(y|H_1)}{f_y(y|H_0)} \underset{H_0}{\overset{H_1}{\lessgtr}} \frac{P_0(C_{10}-C_{00})}{P_1(C_{01}-C_{11})} \tag{1.26}$$

The ratio of $f_y(y|H_1)$ over $f_y(y|H_0)$ is called the likelihood ratio and is denoted $\Lambda(y)$ that is :

$$\Lambda(y) = \frac{f_y(y|H_1)}{f_y(y|H_0)} \tag{1.27}$$

The likelihood statistic $\Lambda(y)$ is a random variable since it is a function of the random variable Y. the threshold is :

$$\eta = \frac{P_0(C_{10}-C_{00}}{P_1(C_{01}-C_{11})} \tag{1.28}$$

Therefore Bayes' criterion , which minimizes the average cost, results in the likelihood ratio test :

$$\Lambda(y) = \frac{f_y(y|H_1)}{f_y(y|H_0)} \underset{H0}{\overset{H_1}{\lessgtr}} \eta \tag{1.29}$$

The threshold value η obtained from Bayes' criterion is the same as the Lagrange multiplier λ in the Neyman-Pearson (N-P) test, where the false alarm probability is set to a specific value $\boldsymbol{\alpha}_0$. If we define the conditional density of $\boldsymbol{\Lambda}$ given that H_0 is true as $f_\Lambda(\lambda|H_0)$, then we can express $P_{f_a} = \alpha_0$ as [14]:

$$P_{f_a} = \int_{z_1} f_y(Y|H_0)\, dy = \int_{\lambda}^{\infty} f_\Lambda(\lambda(y)|H_0)\, dy \tag{1.30}$$

If the probability of rejecting H_0 in a test is exactly α_0 then it is referred to as the most powerful test of level α_0

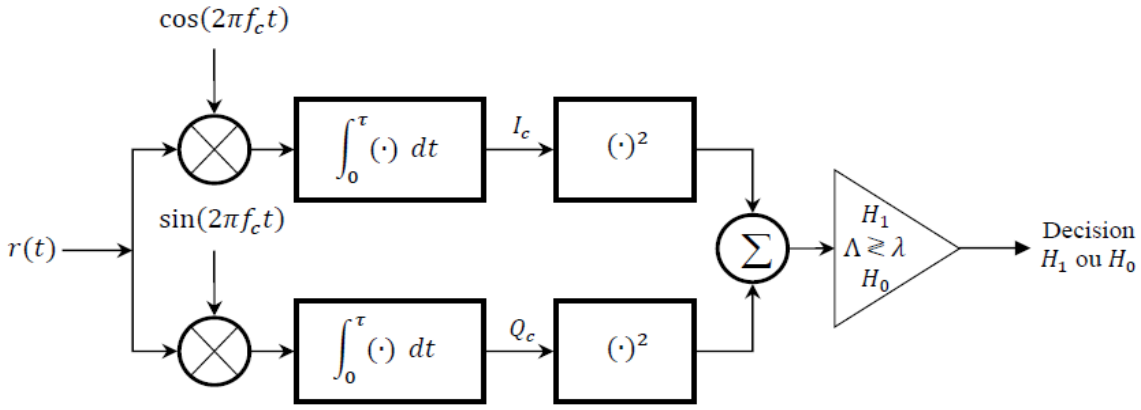

Figure I.9: Optimal Neyman-Pearson quadratic detector

I.6. CFAR detection

In the case of homogeneous clutter, the M samples $x_1, x_2, \ldots\ldots\ldots, x_M$ in the M neighboring cells of the reference window of the CFAR detector are statistically independent and identically distributed (iid) and are independent of the CUT statistic Z_0. A statistical test, denoted Z, is formed from the samples $x_1, x_2, \ldots\ldots\ldots, x_M$ representing an estimate of the average power level of the clutter in the CUT. This estimate is multiplied by a thresholding constant T, which is chosen to guarantee a certain desired false alarm probability, $P_{fa}(T) = \alpha_0$. This results in an adaptive detection threshold.

To decide on the presence or absence of a target in the CUT, the content of the latter, denoted Z_0, is compared to the adaptive threshold according to the following binary decision rule [15, 16, 17]:

$$\text{Decision}=\begin{cases} Target\ present, & T_0 > \alpha T \\ Target\ absent, & T_0 \leq \alpha T \end{cases}$$

$$Z_0 \underset{H_0}{\overset{H_1}{\lessgtr}} TZ \tag{1.31}$$

To assess the performance of any CFAR detector, we often use two key metrics:

- Probability of Detection (Pd)
- Probability of False Alarm (Pfa)

The detection threshold is calculated based on the probability density functions (pdfs) of the two statistics:

$Z_0|H_0$ and Z. To evaluate the performance of a CFAR detector, the false alarm probability p_{f_a} and the detection probability p_d are commonly used. The pdfs of the statistical test Z and the content of the Cell Under Test (CUT), Z_0, under the two hypotheses H_0 and H_1, respectively, are used to compute p_{f_a} and p_d, as follows [14].

$$P_{f_a} = Pr(Z_0 > TZ|H_0) = \int_0^{\infty}\left[\int_{TZ}^{\infty} f_{z_0|H_0}(z_0|H_0)\, dz_0\right] f_Z(Z)dz \tag{1.32}$$

And

$$p_d = Pr(Z_0 > TZ|H_1) = \int_0^{\infty}\left[\int_{TZ}^{\infty} f_{z_0|H_1}(z_0|H_1)\, dz_0\right] f_Z(Z)dz \tag{1.33}$$

It is difficult to determine the probability density functions (PDFs) of the statistics Z, $Z_0|H_1$, which makes it challenging to calculate the false alarm probability and detection probability.

In practice, the user specifies the desired false alarm probability, P_{fa} , denoted as α_0 , and the detection threshold value is deduced accordingly.

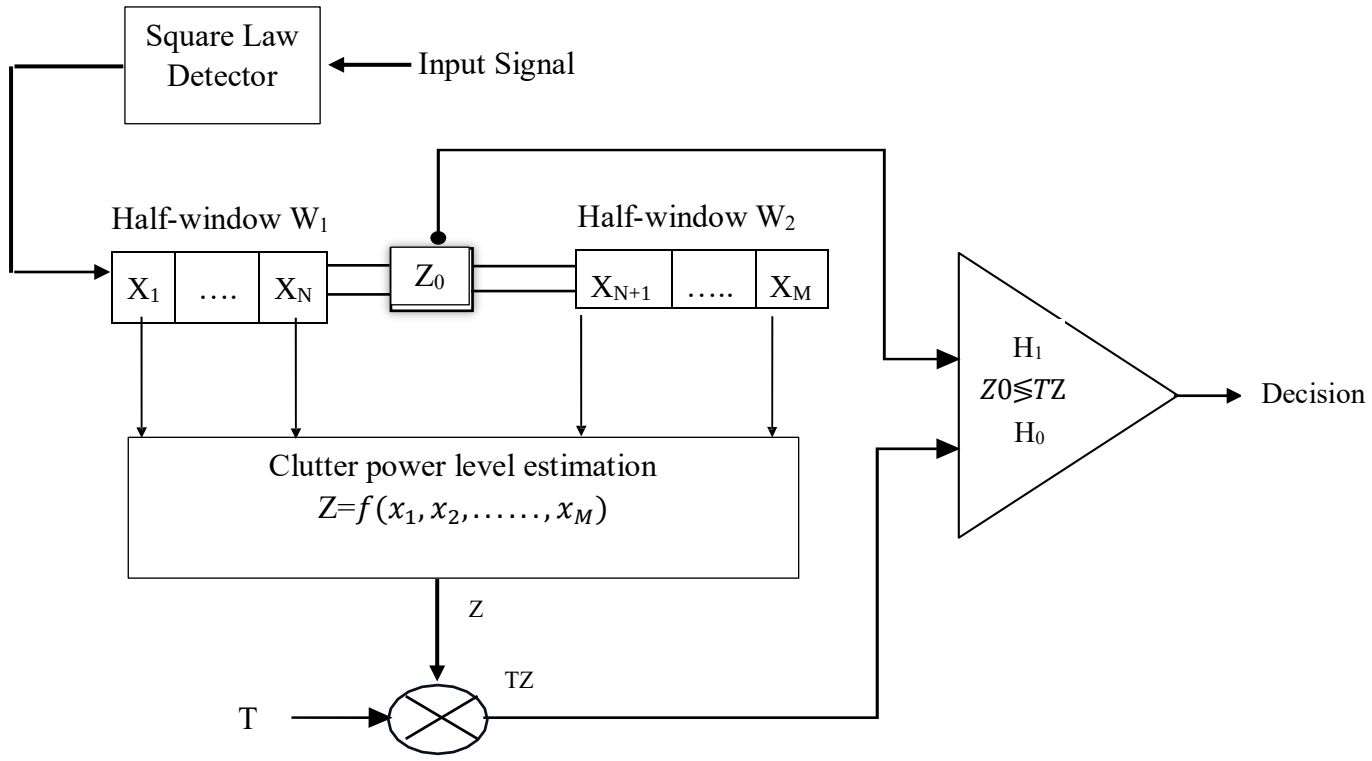

Figure I.10: Typical CFAR detection processor

I.7. Conclusion

In summary, identifying signals within noise presents a significant challenge in numerous signal processing applications. The capability to accurately discern faint signals amidst noise is essential across various domains, such as radar. Crafting efficient algorithms for signal detection in noisy environments necessitates a careful trade-off between sensitivity and specificity, often leveraging distinct statistical and spectral characteristics of both the signal and noise. Progress in this field holds the promise of unlocking new possibilities and enhancing performance across multiple applications.

Chapter II: CFAR Detection in Homogenous Gamma-Distributed Clutter

II.1. Introduction

In this chapter, we examine and analyze CFAR detection in homogeneous Gamma-distributed (GM) clutter. Specifically, we introduce and study three Well-Known CFAR processer:

- Cell-Averaging(CA) CFAR.
- Greatest-Of(GO) CFAR .
- Smallest-Of(SO) CFAR.

As part our analysis, We provide a fundamental understanding of each detector's functioning, along with the corresponding probabilities of false alarm P_{fa} and detection P_d

II.2. Statistics of the CUT

In radar detection, the signal within the Cell Under Test (CUT) is analyzed to determine the presence or absence of a target. This analysis is typically framed as a binary hypothesis testing problem, where the signal behavior is characterized under two distinct hypotheses:

- H_0 (Null Hypothesis): The CUT contains only clutter echoes (C), representing background noise with no target present.

  Modeled as: $f_{H_0}(x) = ClutterPDF(e.g., Gamma, pareto)$

- H_1 (Alternative Hypothesis): The CUT contains both clutter echoes (C) and a target signal return (s), indicating the presence of a target. Modeles as : $f_{H_1}(x) = f_{target+clutter}(x)$

To model this scenario, we assume that the radar system is equipped with a square-law detector before applying Constant False Alarm Rate (CFAR) processing. The statistical distribution of the received signal in the CUT depends on the nature of clutter and target reflections. In many practical cases, clutter is modeled using distributions such as Rayleigh, Weibull, K-distributed, or log-normal. Meanwhile, the target return may follow a Rician or Swerling model, depending on its fluctuation characteristics.Thus, the CUT's content consists either of clutter echoes only or a combination of clutter echoes and target signal returns.

The objective of the detection process is to maximize the probability of target detection while maintaining a constant false alarm rate. This is achieved through adaptive thresholding techniques such as CFAR. The statistical characterization of the CUT's content plays a crucial role in optimizing detection performance under varying environmental conditions. Therefore, the detection problem can be formulated as a binary hypothesis testing problem, which may be expressed as follows [13] [17]:

$$H_0 \text{ (Clutter only): } Z_0 = X \tag{2.1}$$

$$H_1 \text{(Target + clutter): } Z_0 = Y + X \tag{2.2}$$

The symbol H_0 represents the null hypothesis, which states that there is no target in the CUT (i.e., only clutter is present in the CUT). Conversely, H_1 represents the alternative hypothesis, which states that both a target and clutter are present in the CUT.

II.2.1. Statistics of the CUT under H_0

We assume that the content of the CUT Z_0 under H_0 is distributed according to the GM-distribution (here there is no target present in the CUT). Thus, the pdf and cdf of Z_0 in this case are given, respectively, by [11] [18]:

$$f_{z_0}(z_0|H_0) = \left(\frac{\beta^\alpha}{\Gamma(\alpha)}\right) z_0^{\alpha-1} exp(-\beta z_0) \tag{2.3}$$

And

$$F_{z_0}(z_0|H_0) = \frac{\gamma(\alpha,\beta z_0)}{\Gamma(\alpha)} \tag{2.4}$$

II.2.2. Statistics of the CUT under H_1

Under the alternative hypothesis H_1, the Cell Under Test (CUT) in CFAR detection contains both clutter/noise and a target signal. Its statistical properties are determined by the combined effects of the target's radar cross-section and the clutter model. Under H_1, the CUT

follows an exponential distribution with mean μ(1+S) where **S** is the target's signal-to-clutter ratio (SCR). This reflects the increased power due to the target's presence [19][20]:

$$f_{H_1}(x) = \left(\frac{1}{\mu(1+S)}\right) exp\left(\frac{-x}{[\mu(1+S)]}\right) \qquad \text{for } x \geq 0 \tag{2.5}$$

is due to both target returns Y and clutter echoes X . Specifically, we assume throughout this dissertation a Swerling I or II fluctuating target whose pdf and cdf are given, respectively, by:

$$f_Y(y;\sigma_Y) = \left(\frac{1}{2\sigma_Y^2}\right) exp\left(\frac{-y}{2\sigma_Y^2}\right) \tag{2.6}$$

Where σ_Y^2 represents the variance of the in-phase and quadrature components of the target signal Y, and $2\sigma_Y^2$ denotes the average power of the target signal.

By utilizing the appropriate models for target signal returns given in (2.6) and the interfering echoes, we can now examine the distribution of Z_0 under hypothesis H_1.
Since the signal in the test cell(CUT) consists of a combination of the target signal and interference modeled by a GM distribution, analytically deriving the probability density function (PDF) of the CUT's content under H_1 is challenging. For a square-law detector, the complex envelope of the target signal **S** is combined with the complex envelope of the interference signal **C**, and the magnitude of the resulting complex signal is squared. Accordingly, the CUT output Z_0 can be modeled as the squared modulus of the resulting complex signal, which can be expressed as [21]:

$$\begin{aligned} Z_0 = |S + C|^2 &= |S|^2 + |C|^2 + 2|S||C|\cos(\varphi) \\ &= Y + X + 2\sqrt{Y}\sqrt{X}\cos(\varphi) \end{aligned} \tag{2.7}$$

where $|.|$ is the complex modulus, $Y = |S|^2$, $X = |C|^2$ and φ is a random variable (rv) uniformly distributed on the interval $[0, 2\pi]$, which represents here the phase between **S** and **C**.

Unfortunately, a closed-form representation for the probability density function (pdf) of Z_0 under hypothesis H_1 cannot be explicitly derived, which significantly complicates the analysis. Therefore, for simplification, we assume that the pdf of the clutter in the Cell Under Test (CUT) is approximated by an exponential distribution with the exact same mean power as that of the GM-distributed clutter.

Accordingly, the content of the CUT under hypothesis H_1 is reduced to the sum of an exponentially fluctuating target and exponentially distributed clutter. This approximation has demonstrated a high degree of accuracy, making it widely adopted in the literature [22]. In this case, the resulting signal in the CUT will also follow an exponential distribution, and its corresponding conditional pdf can be expressed as follows:

$$f_{Z_0}(z_0|H_1) = \left(\frac{1}{2\sigma_X^2+2\sigma_Y^2}\right) exp\left(\frac{-Z_0}{2\sigma_X^2+2\sigma_Y^2}\right) \quad (2.8)$$

where $2\sigma_X^2 = \alpha/\beta$ is the mean power of GM-distributed clutter in the reference cells, and $2\sigma_Y^2$ is the mean power of the exponentially fluctuating target. Now, the signal-toclutter ratio (SCR) can be defined as:

$$\text{SCR}=\frac{2\sigma_Y^2}{2\sigma_X^2} = \frac{2\sigma_Y^2}{\alpha/\beta} \quad (2.9)$$

Hence, the pdf and cdf of $Z_0|H_1$ can be given in terms of SCR, respectively, by

$$f_{Z_0}(z_0|H_1) = \left(\frac{\beta}{\alpha(1+SCR)}\right) exp\left(\frac{-\beta Z_0}{\alpha(1+SCR)}\right) \quad (2.10)$$

And

$$f_{Z_0}(z_0|H_1) = 1 - exp\left(\frac{-\beta Z_0}{\alpha(1+SCR)}\right) \quad (2.11)$$

II.3. Optimal fixed threshold detector

The optimal fixed threshold detector balances detection probability (P_d) and false alarm rate (P_{fa}) under known noise/clutter statistics, typically derived using the Neyman-Pearson optimal detector for detecting a target in a homogenous background with parameters, which are known a priori (i.e., known power) uses a fixed detection threshold, λ. Unlike adaptive CFAR methods, it assumes stationary noise characteristics, To determine the presence of the target, the signal value Z_0 in the CUT is compared simply to λ, according to the following decision rule

$$\begin{matrix} H_1 \\ Z_0 \lessgtr TZ \\ H_1 \end{matrix} \quad (2.12)$$

II.3.1. P_{fa} of the optimal fixed threshold detector

The threshold T is chosen such that the false alarm probability is constrained to a predefined value, α. For Gaussian noise, this can be expressed as:

$$P_{fa} = \int_T^{\infty} f_{H_0}(x)dx = \alpha \tag{2.13}$$

In the absence of a target in the Cell Under Test (CUT) (i.e., under H_0), the random variable Z_0 follows a Gamma-Mixture (GM) distribution with shape parameter α and scale parameter β. Therefore, the false alarm probability of the optimal detector (P_{fa}^{Op}) can be expressed as

$$\begin{aligned} P_{fa}^{Op} &= Pr(Z_0 > \lambda|H_0) = \int_{\lambda}^{\infty} f_{Z_0}(z_0|H_0)\, dz_0 \\ &= 1 - f_{Z_0}(\lambda|H_0) = 1 - \frac{\gamma(\alpha,\beta\lambda)}{\Gamma(\alpha)} \end{aligned} \tag{2.14}$$

In order to obtain the value of the fixed threshold λ of the optimal detector, for a desired $P_{fa} = \alpha_0$, equation (3.12) must be inverted numerically.

II.3.2. P_d of the optimal fixed threshold detector

The probability of detection (P_d) for an optimal fixed threshold detector is derived under the Neyman-Pearson criterion, assuming perfect knowledge of noise/clutter statistics. It provides a theoretical upper bound for detection performance, which adaptive CFAR detectors approach asymptotically with large reference windows.

For a radar system with exponentially distributed clutter (Rayleigh envelope), the optimal P_d

$$P_d^{Op} = \left[P_{fa}^{Op}\right]^{1/1+s} \tag{2.15}$$

In the presence of a target in the CUT, $Z_0|H_0$ follows the exponential distribution defined by (2.10). Therefore, the probability of detection of the optimal detector (P_d^{Op}) can be determined by

$$\begin{aligned} P_d^{Op} &= Pr(Z_0 > \lambda|H_1) = \int_{\lambda}^{\infty} f_{Z_0}(z_0|H_1)\, dz_0 \\ &= 1 - f_{Z_0}(\lambda|H_1) = exp\left(-\frac{\beta\lambda}{\alpha(1+SCR)}\right) \end{aligned} \tag{2.16}$$

II.4 Cell Averaging CFAR detector:

The Cell-Averaging Constant False Alarm Rate (CA-CFAR) detector is one of the most well-known adaptive thresholding detectors. The calculation of the decision threshold is obtained from the arithmetic mean of the values within the surrounding reference windows. In the case of a statistically uniform and Gaussian-distributed interference, where the interference samples are independent and identically distributed (IID), the CA-CFAR detector exhibits high detection efficiency and approaches the Neyman-Pearson optimal detector if the number of interference samples is sufficiently large. The CA-CFAR detection methodology was initially formulated by Barkat and Varshney [22, 23]. They investigated the problem of detecting a Swerling model I target**,** embedded in additive white Gaussian noise (AWGN) with an unknown power level. For a given target signal-to-noise ratio (SNR), which remains consistent across all distributed local detectors, and assuming a predetermined fusion strategy at the centralized data fusion unit, they derived the optimal threshold scaling factors for each detector and formulated an expression for the overall detection probability at the fusion center.

In this paragraph, we analyze the performance of the Cell Averaging (CA) Constant False Alarm Rate (CFAR) detector in the presence of Gamma Mixture (GM)-distributed clutter. The schematic diagram of the CA-CFAR detector is shown in Figure 2.1 [22].

Consider a set $\{X_i : i = 1, 2, \dots, 2N\}$ of $2N$ independent and identically distributed (iid) GM random variables, representing $2N$ radar clutter samples within the reference window of a given CFAR detector. For the CA-CFAR algorithm, the decision rule is formulated as follows [24].

$$Z_0 \underset{H_1}{\overset{H_1}{\lessgtr}} TZ \tag{2.17}$$

Where $Z_{CA} = \sum_{i=1}^{2N} X_i$ is a sufficient statistic of clutter power level. Whose pdf can be expressed, according to [21].by

$$\mathrm{f}_{Z_{CA}} = \frac{\beta^{2N\alpha}}{\Gamma(2N\alpha)} Z^{2N\alpha-1} e^{-\beta z} \tag{2.18}$$

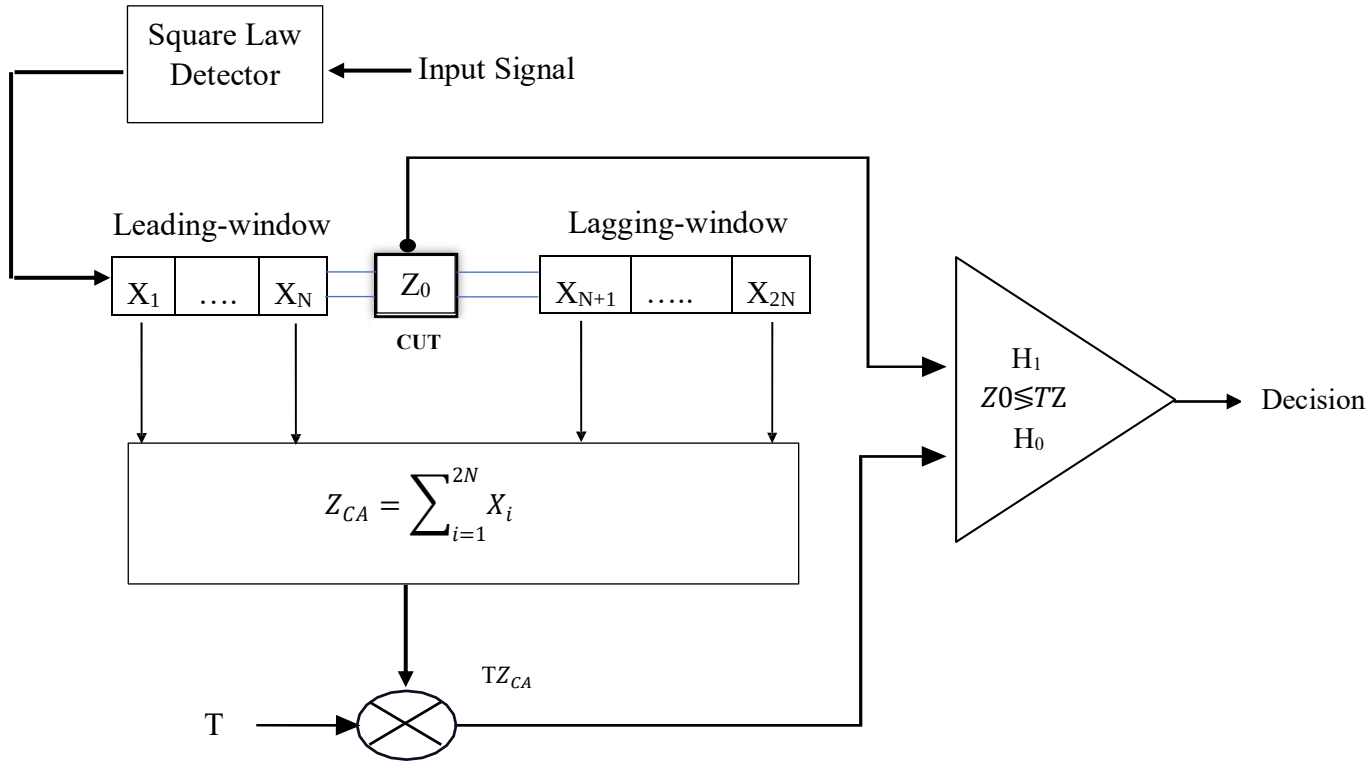

Figure II.1: Block diagram of the CA-CFAR detector

II.4.1. P_{fa} of the CA-CFAR detector

The probability of false alarm (P_{fa}) for a CA-CFAR (Cell-Averaging Constant False Alarm Rate) detector is determined by its threshold factor (α) and the number of reference cells (N). Under homogeneous Gamma-distributed clutter (or exponential noise, a special case of Gamma).

The false alarm probability (P_{fa}) of the CA-CFAR detector can be obtained by replacing (2.3) or (2.4) and (2.17) into (1.32), is derived as [17]

$$P_{\text{fa}}^{CA} = \frac{\Gamma(\alpha(2N+1))T^{\alpha}}{\Gamma(2N\alpha+1)\Gamma(\alpha)(1+T)^{\alpha(2N+1)}}\,{}_2\text{F}_1(1, \alpha(2\text{N}+1); 2\text{N}\alpha+1; \frac{1}{1+T}) \qquad (2.19)$$

Where ${}_2F_1$ (..,…..,..) denotes the Gauss hypergeometric function [24].

II.4.2. P_d of the CA-CFAR detector

The probability of detection (P_d) for a CA-CFAR (Cell-Averaging Constant False Alarm Rate) detector depends on the signal-to-clutter ratio (SCR), the number of reference cells (N), and

the design probability of false alarm (P_{f_a}). In homogeneous Gamma-distributed clutter (or exponential noise, a special case of Gamma). The detection probability (P_d) of the CA-CFAR detector can be obtained by replacing (2.10) or (2.11) and (2.17) into (1.33) as follows

$$P_{\mathrm{d}}^{CA} = pr(Z_0 > TZ_{CA}|H_1)$$

$$= \int_0^{\infty}\left[\int_{Tz}^{\infty} f_{z_0}(z_0|H_1)\, dz_0\right] f_{ZCA}(Z)dz$$

$$= 1 - \int_0^{\infty}\left(1 - exp\left(\frac{\beta Tz}{\alpha(1+SCR)}\right)\right) f_{ZCA}(Z)dz \qquad (2.20)$$

$$= \frac{1}{\Gamma(2N\alpha)}\int_0^{\infty} z^{2N\alpha-1}\, exp\left(-1\left(1+\frac{T}{\alpha(1+SCR)}\right)z\right)dz$$

This last integral can be solved using equation 3.381.4 of [25], which yields the following closed-form approximation for the P_d of the CA-CAFR detector

$$P_{\mathrm{d}}^{CA} = \left(1+\frac{T}{\alpha(1+SCR)}\right)^{-2N\alpha} \qquad (2.21)$$

II.5. Greatest of CFAR detector

Herein, we will analyze the performance of the Greatest Of (GO) CFAR detector in presence of GM-distributed clutterThe Greatest-Of CFAR (GO-CFAR) detector is designed to mitigate false alarms at clutter edges by conservatively estimating the noise floor, at the expense of reduced detection sensitivity in homogeneous environments compared to CA-CFAR.

In many real-world situations, clutter is not uniformly distributed. This may be due to the presence of a clutter edge or interfering targets at the reference cells. In this case, the clutter is said to be heterogeneous. The detection threshold is affected and produces an increase in false alarms. To control the regulation of the $P_{f_a}$the GO-CFAR detector was proposed where the cells of the reference window are separated into two sub-windows upstream and downstream of the cell under test. The contents of each half-window are summed, and the larger of the two is then used to estimate the clutter power. The GO-CFAR detector showed better performance when a clutter edge is present in one of the two half-windows. However, when the target is embedded in the half-

window containing only thermal noise or when targets are present, the clutter power is significantly higher. interfering, the detection performance of the GO-CFAR detector degrades significantly . The block diagram of the GO-CFAR detector is shown in Figure 2.2. The decision rule of this detector is defined as follows [11, 26]

$$Z_0 \underset{H_1}{\overset{H_1}{\lessgtr}} TZ_{GO} \tag{2.22}$$

Where $Z_{GO} = Max(U,V)$, and $U = \sum_{i=1}^{N} X_i$ and $U = \sum_{i=N+1}^{2N} X_i$ are two sufficient statistics of clutter power level, whose pdfs and cdfs can be expressed, respectively, by

$$f_U(Z) \triangleq f_V(Z) = \frac{\beta^{N\alpha}}{\Gamma(N\alpha)} z^{N\alpha-1} exp(-\beta z) \tag{2.23}$$

$$f_U(Z) \triangleq f_V(Z) = \frac{\gamma(N\alpha,\beta z)}{\Gamma(N\alpha)} \tag{2.24}$$

According to [14], the pdf of $f_{Z_{GO}}$ can be calculated as follows

$$f_{Z_{GO}}(z) = 2f_U(Z)F_V(Z) \triangleq 2f_V(Z)F_V(Z) \tag{2.25}$$

Which yields

$$f_{Z_{GO}}(z) = \frac{2\beta^{N\alpha}}{\Gamma^2(N\alpha)} z^{N\alpha-1} \gamma(N\alpha,\beta z) exp(-\beta z) \tag{2.26}$$

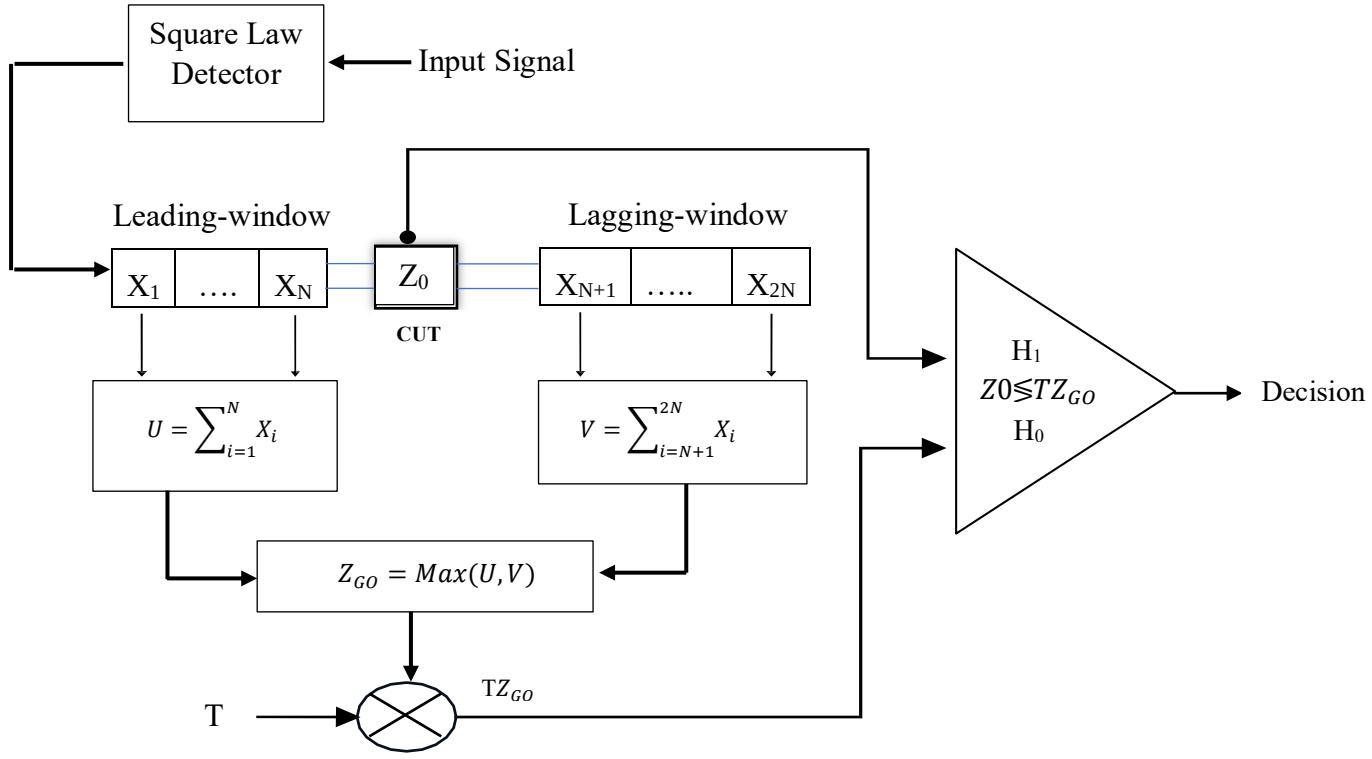

Figure II.2: Block diagram of the GO-CFAR detector

II.5.1. P_{fa} Of The GO-CFAR Detector:

The probability of false alarm (P_{fa}) for the GO-CFAR (Greatest-Of CFAR) detector is derived under homogeneous Gamma-distributed clutter and involves a closed-form expression that accounts for its conservative thresholding strategy. GO-CFAR selects the larger of two reference window averages to avoid underestimating noise power at clutter edges.

The false alarm probability (P_{fa}) of the GO-CFAR detector can be obtained by replacing (2.3) or (2.4) and (2.25) into (1.31), and it can be given as [7]

$$P_{fa}^{GO} = \frac{2}{\Gamma^2(N\alpha)}\left[\frac{\Gamma\left(\frac{1}{2}\right)\Gamma(2N\alpha)\Gamma(N\alpha)}{2^{2N\alpha}\Gamma\left(N\alpha\frac{1}{2}\right)} - \frac{\Gamma\big(\alpha(2N+1)\big)T_{GO}^{\alpha}}{N\alpha^2\Gamma(\alpha)(2+T_{GO})^{\alpha(2N+1)}}\right] \times F_2\left(\alpha(2N+1),1,1;N\alpha+1;\frac{1}{2+T_{GO}},\frac{T_{GO}}{2+T_{GO}}\right) \quad (2.27)$$

Where F_2 (a,b ,·;·,·;·,) denotes the Gauss hypergeometric function [24, 27].

II.5.2. P_d of the GO-CFAR detector

The probability of detection (P_d) for the GO-CFAR (Greatest-Of CFAR) detector is derived under homogeneous Gamma-distributed clutter and depends on the signal-to-clutter ratio (SCR), threshold factor (α), and the number of training cells (N). GO-CFAR selects the greater of two reference window averages to set the threshold, introducing a trade-off between false alarm suppression and detection sensitivity. Now, the detection probability (P_d) of the GO-CFAR detector can be obtained by replacing (2.10) or (2.11) and (2.25) into (1.33)

$$\begin{aligned} P_{\mathrm{d}}^{GO} &= pr(Z_0 > TZ_{GO}|H_1) \\ &= \int_0^{\infty}\left[\int_{TZ}^{\infty} f_{z_0}(z_0|H_1)\,dz_0\right] f_{z_{GO}}(Z)dz \\ &= 1 - \int_0^{\infty}\left(1 - exp\left(-\frac{\beta Tz}{\alpha(1+SCR)}\right)\right) f_{z_{GO}}(Z)dz \\ &= \frac{2}{\Gamma^2(N\alpha)}\int_0^{\infty} z^{N\alpha-1}\, exp\left(-1\left(1+\frac{T}{\alpha(1+SCR)}\right)z\right)dz \end{aligned} \tag{2.28}$$

This last integral can be solved using equation 3.381.4 of [25], which yields the following closed-form approximation for the P_d of the GO-CAFR detector

$$P_{\mathrm{d}}^{GO} = \frac{2\Gamma(2N\alpha)}{N\alpha\Gamma^2(N\alpha)\left(2+\frac{T}{\alpha(1+SCR)}\right)^{2N\alpha}}\,{}_2\mathrm{F}_1\left(1,2N\alpha; N\alpha+1; \frac{1}{2+\frac{T_{GO}}{\alpha(1+SCR)}}\right) \tag{2.29}$$

II.6. Smallest of the CFAR detector

The SO-CFAR algorithm, a variant of traditional CFAR (Constant False Alarm Rate) techniques, is recognized for its superior detection capabilities in non-homogeneous environments. Specifically, it is designed to operate effectively in scenarios where clutter or interference may exist asymmetrically around the Cell Under Test (CUT). Unlike other CFAR variants, SO-CFAR selects the minimum value from a set of reference cells, thereby offering robustness in environments where interference affects only one side of the CUT.

Despite its favorable detection performance, SO-CFAR is known to suffer from an elevated false alarm rate, which has limited its adoption and exploration in the existing literature. To address this

limitation, we investigate the use of a neural network trained on SO-CFAR detections. Our results demonstrate that this approach can significantly reduce the false alarm rate while maintaining a high probability of detection, thereby improving overall radar system performance in cluttered and challenging environments.

For this detector, the clutter power estimate, denoted by z_{SO}, is simply the smallest of both sums U and V, which are defined previously

(i.e. $z_{SO} = min(U,V)$). Its corresponding pdf can be calculated, in the case of homogenous clutter

$$f_{z_{so}}(z) = 2f_U(z) - f_{z_{Go}}(z) = 2f_V(z) - f_{z_{Go}}(z) \tag{2.30}$$

Therefore, by replacing (2.23) and (2.26) into (2.30), the pdf of the statistic z_{SO}, in the ca se of GM clutter, can be expressed as

$$f_{z_{so}}(z) = \frac{2}{\Gamma^2(N\alpha)\beta^{N\alpha}} Z^{N\alpha-1} \exp\left(\frac{-Z}{\beta}\right) - f_{z_{Go}}(z) \tag{2.31}$$

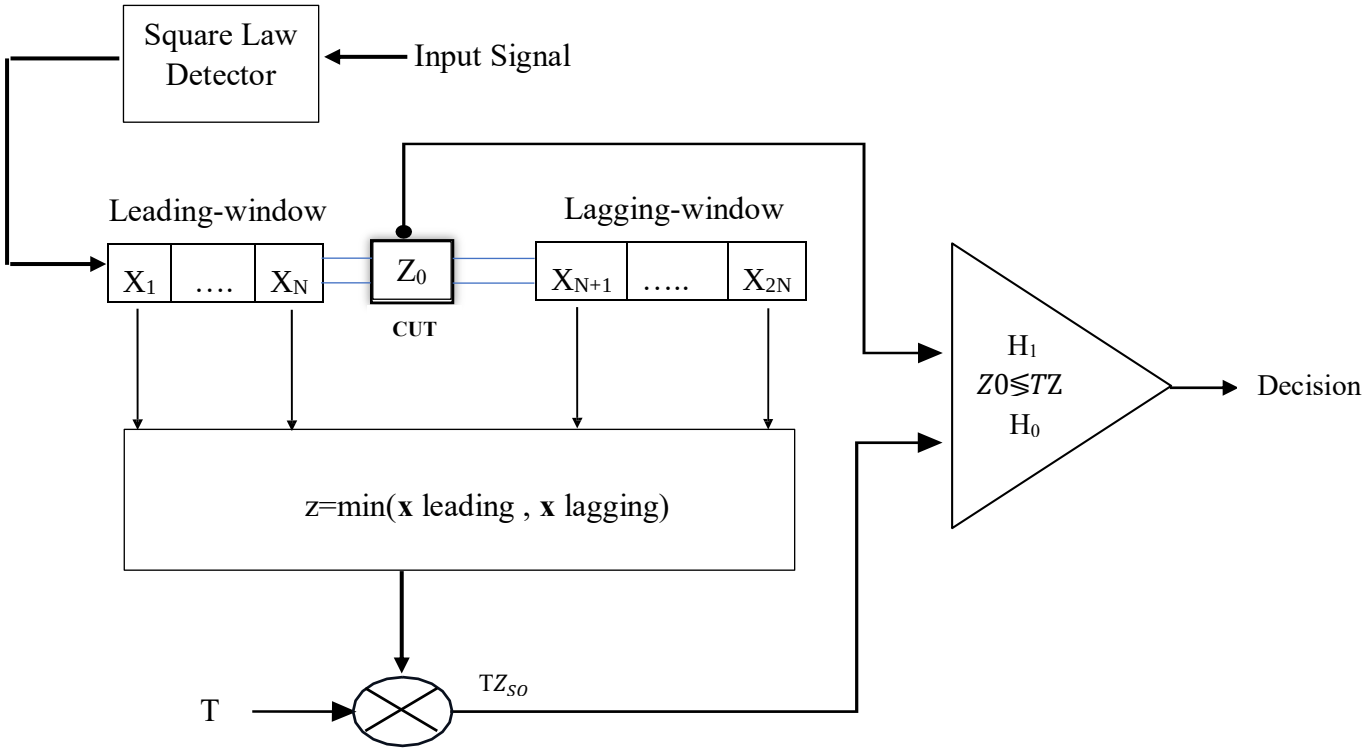

Figure II.3: Block diagram of the SO-CFAR detector

II.6.1. P_{fa} of the SO-CFAR detector

For the SO-CFAR detector, the clutter level estimation z uses the minimum of two local independent estimators x for leading window and y for lagging window. Thus, the PDF of z is given as a function of the PDF and the CDF of x by

Herein, we present the performance of the SO-CFAR detector operating over a homogeneous GM clutter. First, the probability of false alarm of this detector (P_{fa}^{SO}) can be easily evaluated by replacing (2.4) and (2.31) into (2.14), which yields

$$P_{fa}^{SO} = \frac{2\Gamma(\alpha(N+1))P_{SO}^{\alpha}}{\Gamma(N\alpha+1)\Gamma(\alpha)(1+T_{SO})^{\alpha(N+1)}}\mathrm{F}_1(1,\alpha(2\mathrm{N}+1);\mathrm{N}\alpha+1;(1+T_{SO})^{-1}) - P_{fa}^{GO}(T_{SO}) \tag{2.32}$$

where T_{SO} is the normalized scaling factor of the SO-CFAR detector, and $P_{fa}^{GO}(T_{SO})$ can be obtained straightforwardly from (2.27) by replacing T_{GO} with T_{SO}. It may be noted here that a multiple pulse version of (2.32) has been already introduced by Baadeche and Soltani (2023).

II.6.2. P_d of the SO-CFAR detector

The corresponding P_d of the SO-CFAR detector (P_d^{SO}) can be achieved using (2.16). The following result holds

where$P_d^{GO}(T_{SO})$ was previously provided in (2.29) just T_{GO} must be replaced by T_{SO}.

The P_d of the SO-CFAR detector can be attained, by replacing (2.11) and (2.31) into (2.16), as follows:

$$\begin{aligned} P_{\mathrm{d}}^{SO} &= pr(Z_0 > TZ_{SO}|H_1) \\ &= \int_0^{\infty}\left[\int_{Tz}^{\infty} f_{z_0}(z_0|H_1)\,dz_0\right] f_{z_{GO}}(Z)dz \\ &= 1 - \int_0^{\infty} F_{z_0}(T_{SO}z_0|H_1) f_{z_{SO}}(z)dz \end{aligned} \tag{2.33}$$

$$P_d^{SO} = 1 - \int_0^{\infty}\left(1 - exp\left(\frac{\beta Tz}{\alpha(1+SCR)}\right)\right) f_{zSO}(Z)dz$$

$$= \frac{2}{\Gamma^2(N\alpha)}\int_0^{\infty} z^{N\alpha-1}\, exp\left(-1\left(1+\frac{T}{\alpha(1+SCR)}\right)z\right) - P_d^{GO}(T = T_{SO})$$

This last integral can be solved using equation 3.381.4 of [25], which yields the following closed-form approximation for the P_d of the SO-CAFR detector

$$P_d^{SO} = 2\left(1+\frac{T}{\alpha(1+SCR)}\right)^{-N\alpha} - P_d^{GO}(T_{SO})$$

$$P_d^{SO} = 2P_d^{CA}(T_{SO}) - P_d^{GO}(T_{SO}) \tag{2.35}$$

II.7. Conclusion

In this chapter, we begin by presenting an overview of Constant False Alarm Rate (CFAR) detection for radar signals embedded in homogeneous clutter modeled by a Gamma distribution. The study then concentrates on the analysis of three widely used Mean-Level CFAR detectors: the Cell Averaging (CA), the Greatest Of (GO), and the Smallest Of (SO) detectors. A particular emphasis is placed on the SO detector due to its relevance in scenarios characterized by localized interference or strong non-homogeneities in the clutter.

For each detector, including the SO, we detail the underlying detection principle and derive the analytical expressions for the Probability of False Alarm (P_{fa}) and the Probability of Detection (P_d). Closed-form expressions for P_{fa} are provided, while approximations are proposed for P_d, particularly in the case of the SO detector, due to the mathematical complexity associated with its detection structure.

The SO detector, which selects the minimum among reference cells for threshold computation, is analyzed in depth. Its performance is evaluated in comparison with the CA and GO detectors, with particular attention to its robustness in the presence of interfering targets or clutter edge effects. A comparative performance analysis of all three detectors will be conducted in the final chapter.

Chapter III: Results and discussion

III.1 introduction

In this final chapter, we evaluate the performance of the previously discussed CFAR (Constant False Alarm Rate) detectors—namely, the CA-CFAR, GO-CFAR, and SO-CFAR—through a series of simulations conducted over homogeneous Gaussian mixture (GM) clutter.

We begin by detailing the parameters employed in our simulations. Following this, we validate the analytical expressions for the threshold multipliers P_{fa} and P_d derived for each detector. This validation is performed through comparison with both existing integral formulations and simulation-based results. Subsequently, we assess and compare the performance of the aforementioned CFAR detectors—CA-CFAR, GO-CFAR, and SO-CFAR—against the optimal fixed-threshold detector. The latter serves as a performance benchmark, given its reliance on prior knowledge of clutter parameters.

Initially, numerical results are presented to validate the accuracy of the proposed analytical expressions—specifically, equations (2.18), (2.20), (2.26), (2.28), (2.31), and (2.33)—for the CA-CFAR, GO-CFAR, and SO-CFAR detectors, respectively. Finally, the detection performance of these CFAR detectors is evaluated and compared to that of the optimal detector

III.2 Simulation parameters

To analyze the performance of the aforementioned CFAR detectors, a series of simulations were conducted. The impact of varying different parameters on the probability of false alarm (P_{fa}) and the probability of detection (P_d) was examined under various simulation scenarios.

The performance evaluation of all detectors was carried out using both analytical results and Monte Carlo (MC) simulations. The number of trials for the MC simulations was set to 10^7, and the generated samples were assumed to be independent and identically distributed (IID) following a Gamma distribution. It is important to note that the MC simulation results were included primarily for validation purposes.

To this end, clutter modeled by a Gamma distribution was simulated using shape parameters α=2, 3, and 5. For each value of α, the size of the CFAR reference window was chosen as 2N=08,12 and 16. Consequently, the resulting data matrix was of size $2N\times10^7$, allowing it to be assimilated into

a CFAR reference window generated 10^7 times. Additionally, the contents of the Cell Under Test (CUT) were also generated 10^7 times under both hypotheses H_0 and H_1.

In all considered scenarios, the simulated Receiver Operating Characteristic (ROC) curves, i.e., P_d versus P_{fa}, were generated using 10^7 Monte Carlo trials. For each detector, the decision rules corresponding to equations (2.16) and (2.21) were implemented, and the respective detection thresholds were estimated accordingly.

To evaluate the detection performance (P_d), the simulations also incorporated a fluctuating target modeled using the Swerling I or II model.

III.3 Validation of P_{fa} and P_d expressions

To assess the accuracy and applicability of the proposed expressions for P_{fa} and P_d, a series of numerical experiments is conducted. Specifically, the exact closed-form solutions for P_{fa} and the approximate expressions for P_d are evaluated and compared against reference results obtained using numerical integration and Monte Carlo simulation techniques. This comparative analysis provides a comprehensive validation of the derived models under various scenarios.

III.3.1 Validation of P_{fa} expressions

We validate the expressions of P_{fa} for Optimal, CA-, GO-, and SO-CFAR detectors. Figures III.1 to III.11 illustrate the evolution of P_{fa} as a function of the scaling factor α for all detectors, respectively. As shown in these figures, all P_{fa} curves are in excellent agreement across the Optimal, CA-, GO-, and SO-CFAR detectors, thereby confirming the validity of our analytical derivations.

Furthermore, Figures III.1 Optimal, Figures III.3 (CA-CFAR), III.6 (GO-CFAR), and III.9 (SO-CFAR) demonstrate that P_{fa}remains stable regardless of the value of β , which confirms the CFAR property of Optimal, CA-, GO-and the SO-CFAR detectors with respect to β . In contrast, Figures III.2, III.4, III.5, III.7, III.8, III.10 and III.11 reveal that the corresponding detectors do not maintain the CFAR property with respect to α and N .

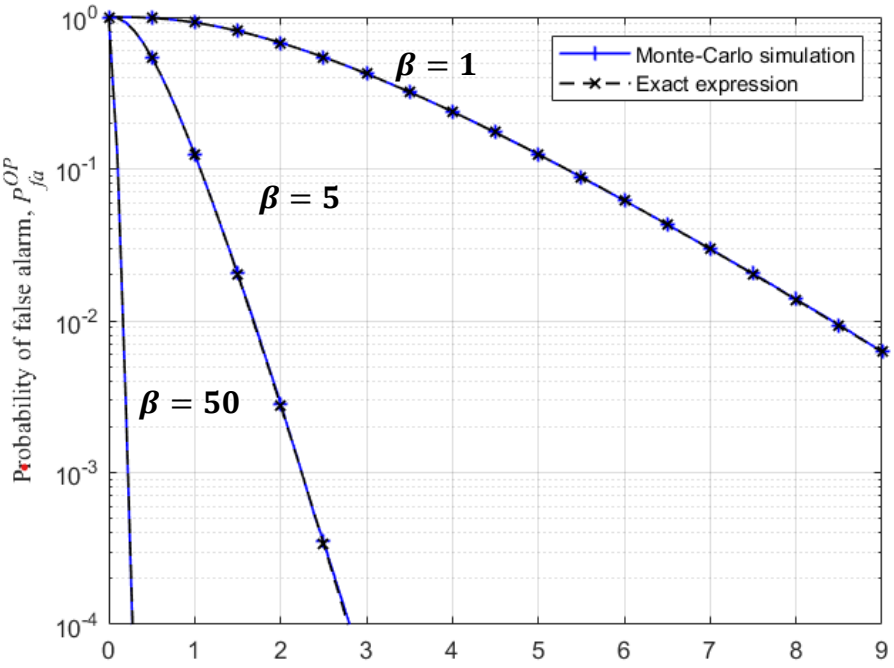

Figure III.1: Probability of False Alarm the Optimal detector against the scaling factor *T* for different values of $\boldsymbol{\beta}$($\boldsymbol{\beta}$ = **1**,**5** and **50**)

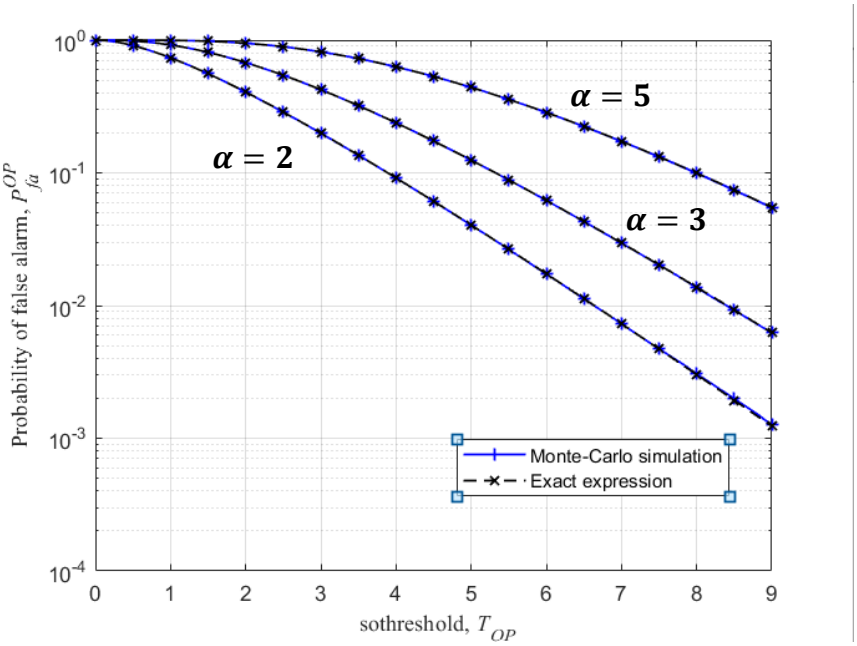

Figure III.2: Probability of False Alarm the Optimal detector against the scaling factor *T* for different values of $\boldsymbol{\alpha}$($\boldsymbol{\alpha}$ = **2**, **3** and **5**)

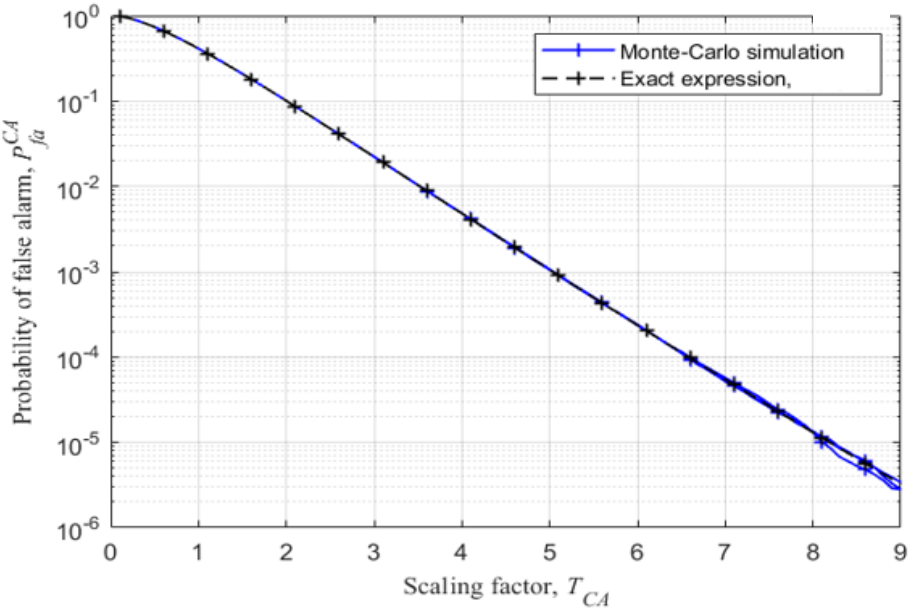

Figure III.3: Probability of False Alarm the CA-CFAR detector against the scaling factor T for different values of $\boldsymbol{\beta}$($\boldsymbol{\beta}$ = **1**,**5** and **50**)

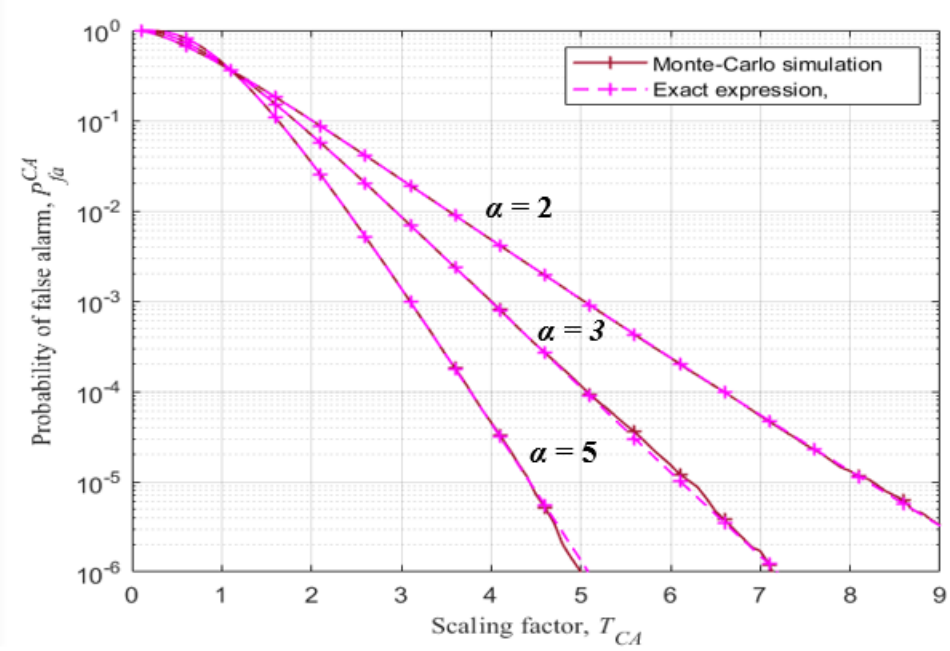

Figure III.4: Probability of False Alarm CA-CFAR detector against the scaling factor T for different values of $\boldsymbol{\alpha}$($\boldsymbol{\alpha}$ = **2**, **3** and **5**)

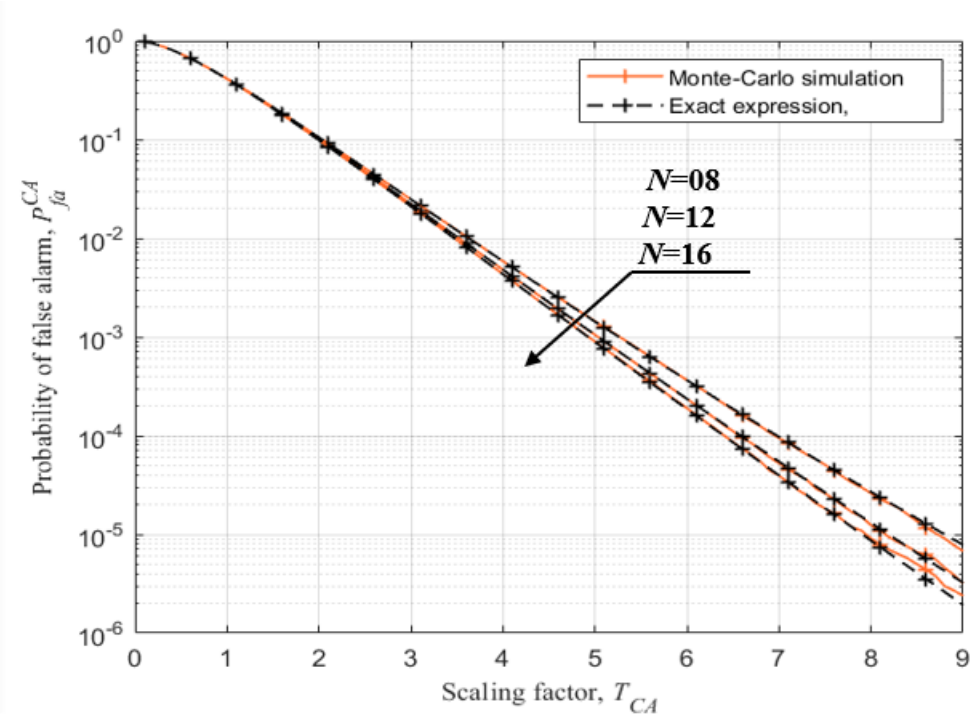

Figure III.5: Probability of False Alarm the CA-CFAR detector against the scaling factor T for different values of N(**N= 8**, **12** and **16**)

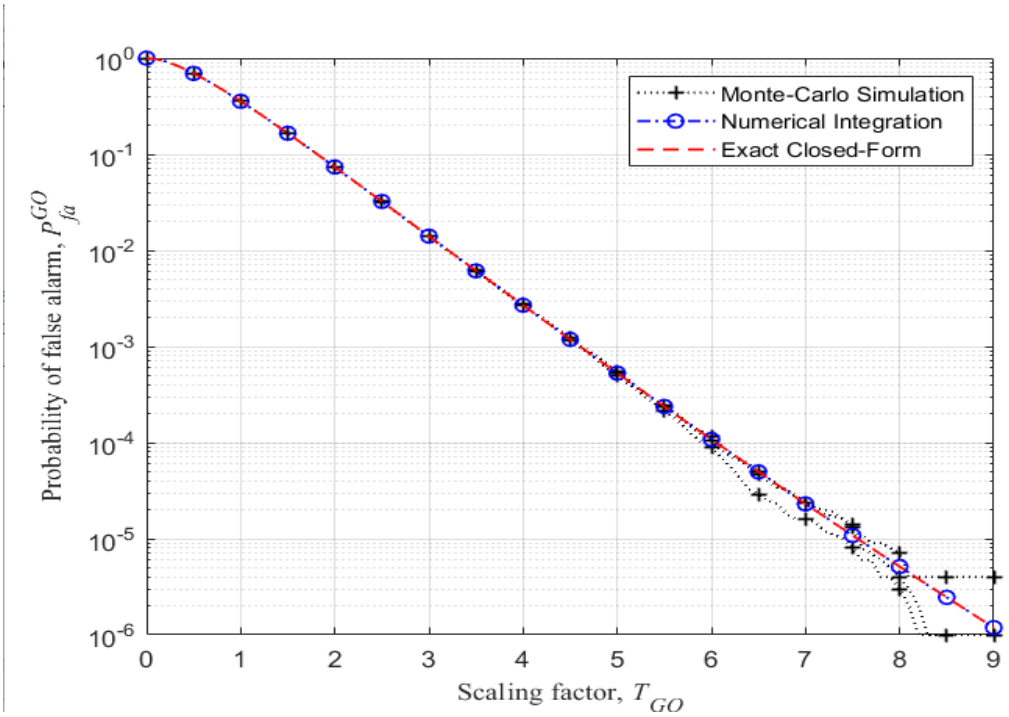

Figure III.6: Probability of False Alarm the GO-CFAR detector against the scaling factor T for different values of β(β = **1**, **5** and **50**)

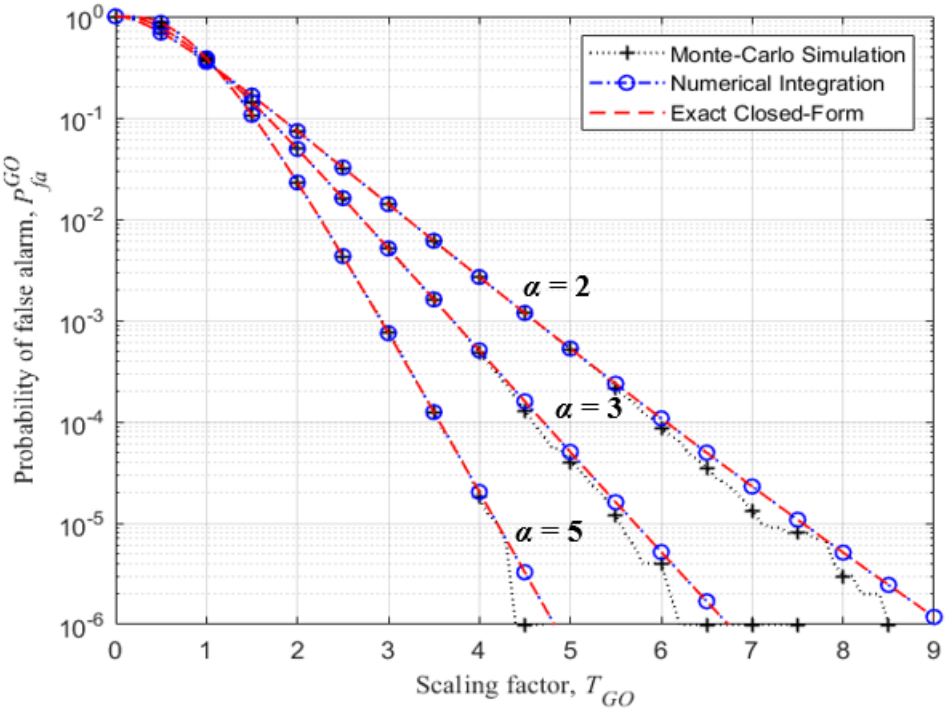

Figure III.7: Probability of False Alarm the GO-CFAR detector against the scaling factor T for different values of $\boldsymbol{\alpha}$($\boldsymbol{\alpha}$ = **2**, **3** and **5**)

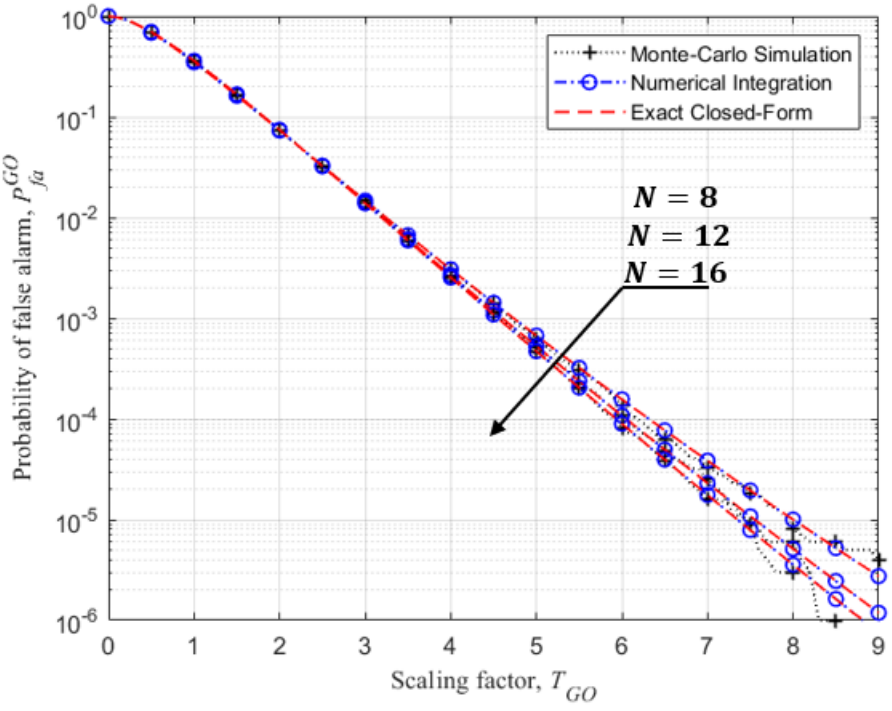

Figure III.8: Probability of False Alarm the GO-CFAR detector against the scaling factor T for different values of $\boldsymbol{N}$($\boldsymbol{N}$ = **8**, **12** and **16**)

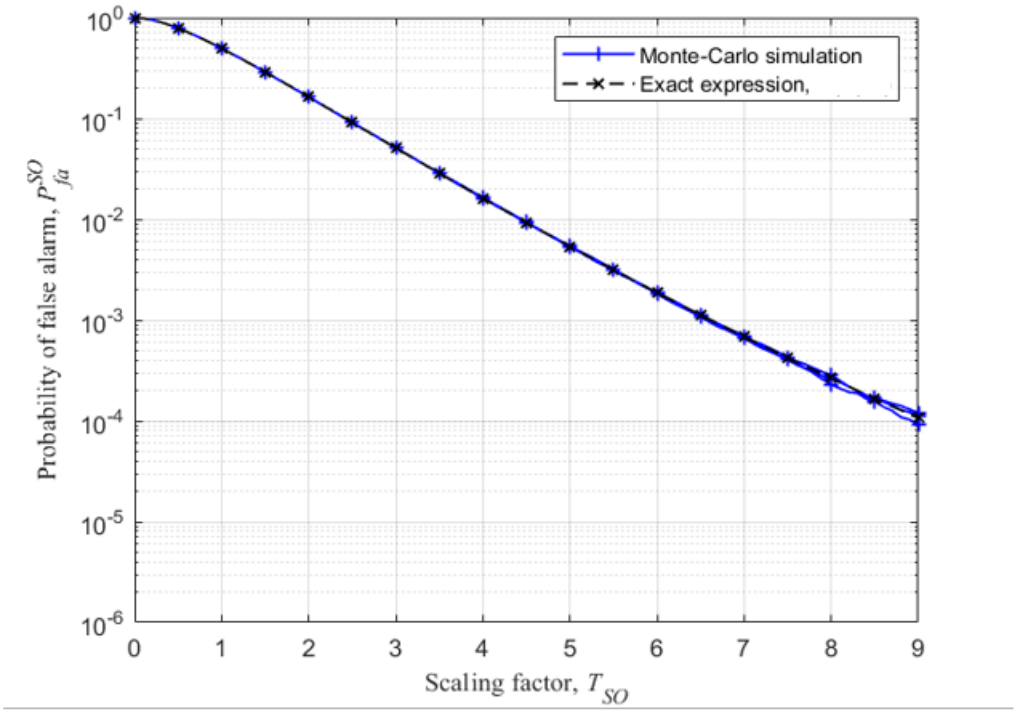

Figure III.9: Probability of False Alarm the SO-CFAR detector against the scaling factor T for different values of $\boldsymbol{\beta}$($\boldsymbol{\beta}$ = **1**, **5** and **50**)

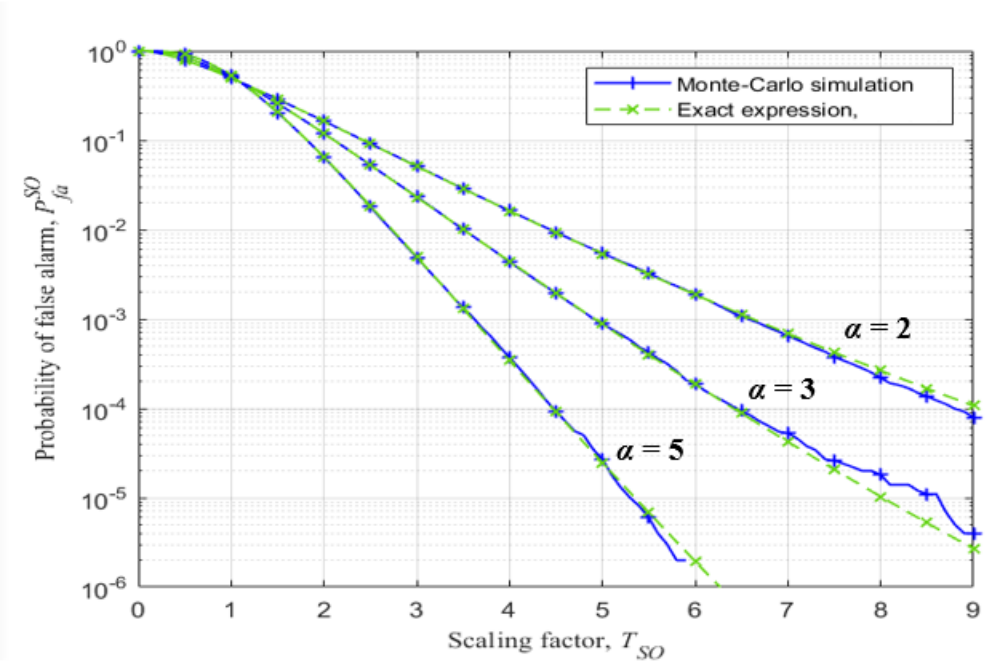

Figure III.10: Probability of False Alarm the SO-CFAR detector against the scaling factor T for different values of $\boldsymbol{\alpha}$($\boldsymbol{\alpha}$ = **2**, **3** and **5**)

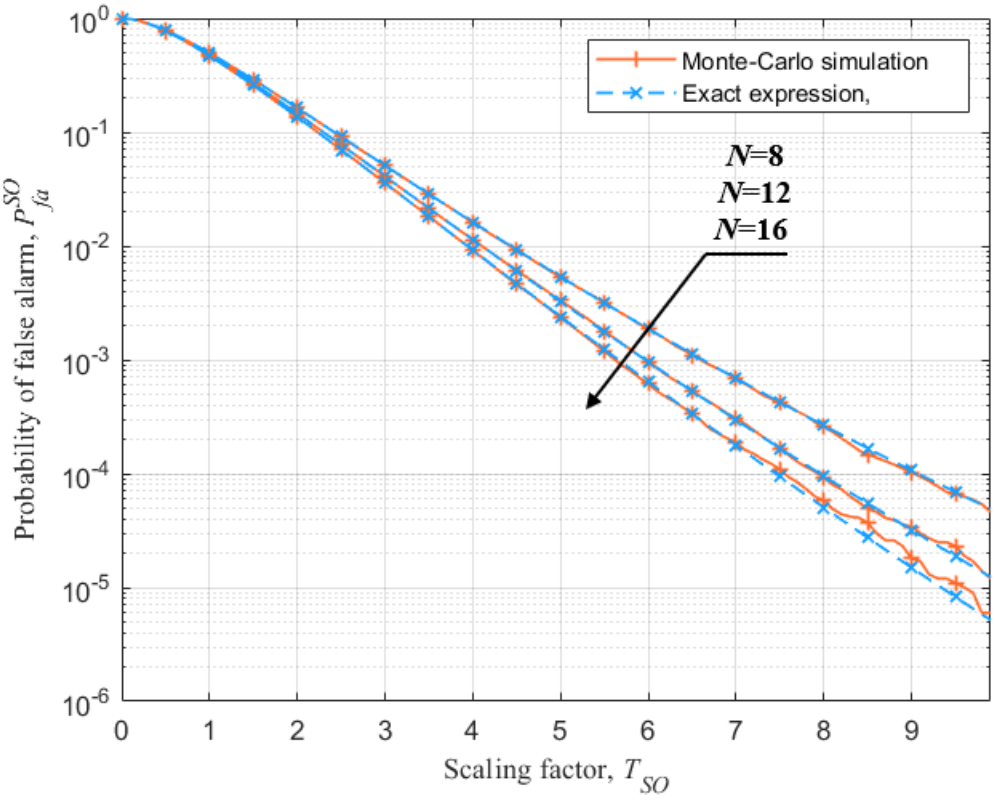

Figure III.11: Probability of False Alarm the SO-CFAR detector against the scaling factor T for different values of $\boldsymbol{N}$($\boldsymbol{N}$ = **8**, **12** and **16**)

III.3.2 Validation of P_d expressions

To evaluate the detection performance, this subsection presents a validation of the proposed approximation expressions for the probability of detection (P_d) for the Optimal, CA-, GO-, and SO-CFAR detectors. The approximated P_d values are compared with those obtained through Monte Carlo simulations.

The detection performance of all detectors is illustrated in Figures III.12 to III.22 In each case, the probability of detection is plotted as a function of the Signal-to-Clutter Ratio (SCR), expressed in decibels (dB). For each estimate of P_d, Monte Carlo simulations were conducted using 10^6 independent trials. The target present in the Cell Under Test (CUT) follows a Swerling I or II model, consistent with the assumptions in [16].

The results clearly demonstrate a strong agreement between the approximated and simulated P_d values across all CFAR detectors considered. This confirms the validity and accuracy of the proposed approximations, especially at relatively high SCR levels.

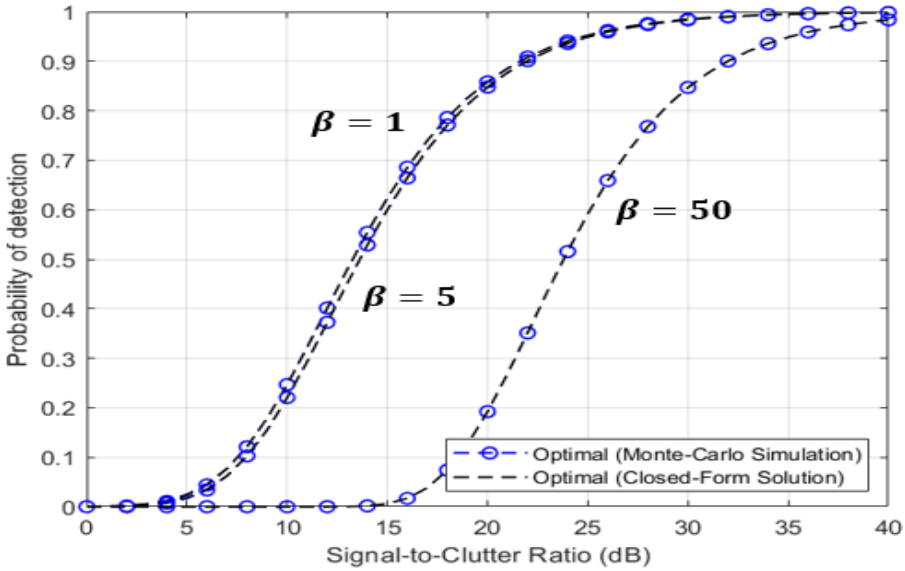

Figure III.12: Probability of detection the Optimal detector against the SCR for $\boldsymbol{\alpha = 3}$ N= 12, $\boldsymbol{P_{fa} = 10^{-4}}$ different values of $\boldsymbol{\beta}$($\boldsymbol{\beta}$ = 1,5 and 50)

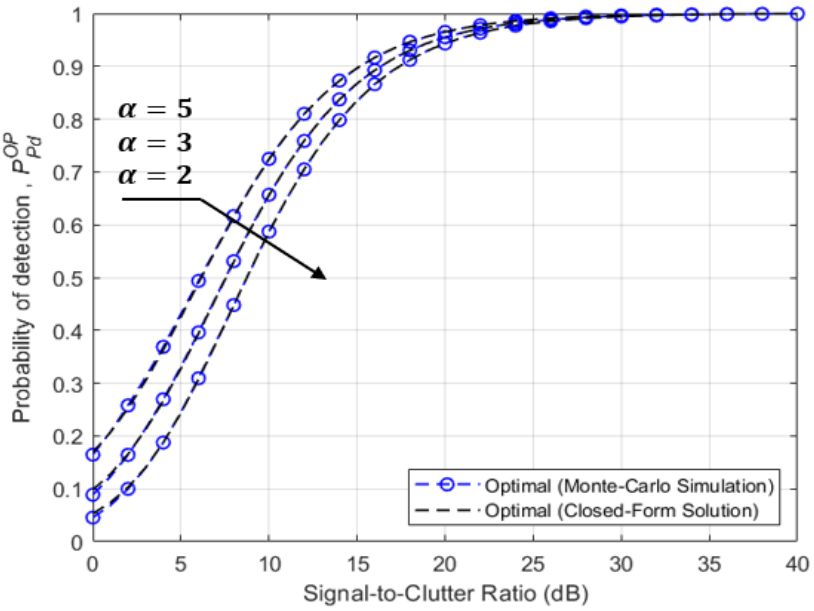

Figure III.13: Probability of detection of Optimal against the SCR for $\boldsymbol{\beta}$ = 1 N=12 $\boldsymbol{P_{fa} = 10^{-4}}$ and different values of $\boldsymbol{\alpha}$($\boldsymbol{\alpha = 2, 3}$ *and* $\boldsymbol{5}$)

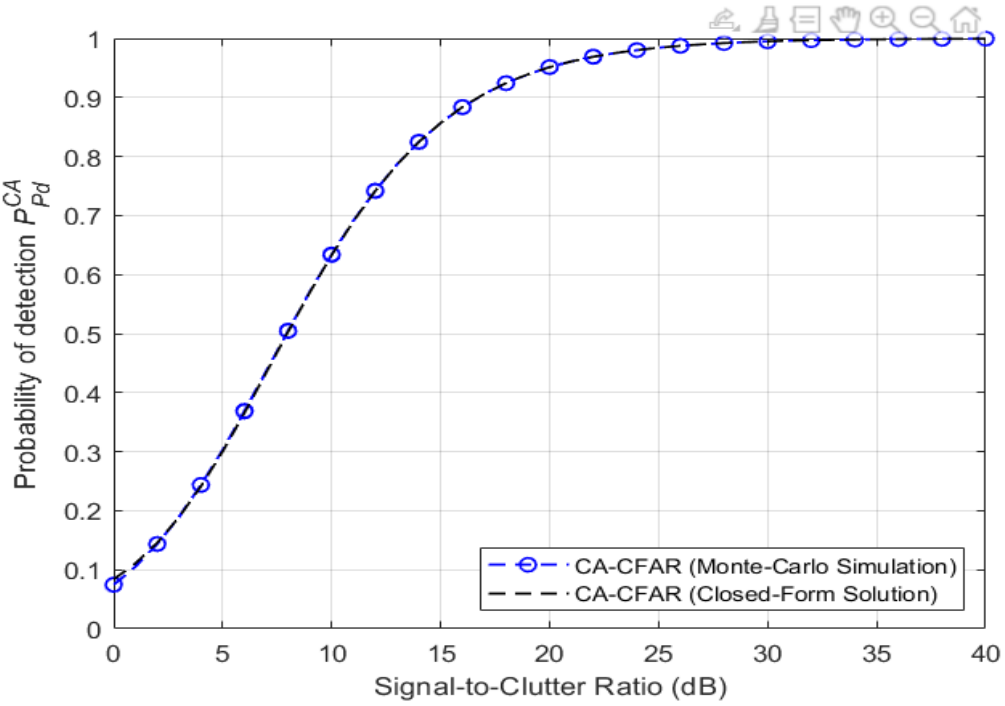

Figure III.14: Probability of detection the CA-CFAR detector against the SCR for $\boldsymbol{\alpha = 3}$ **N= 12**, $\boldsymbol{P_{fa} = 10^{-4}}$ different values of $\boldsymbol{\beta}$($\boldsymbol{\beta}$ = **1**,**5** and **50**)

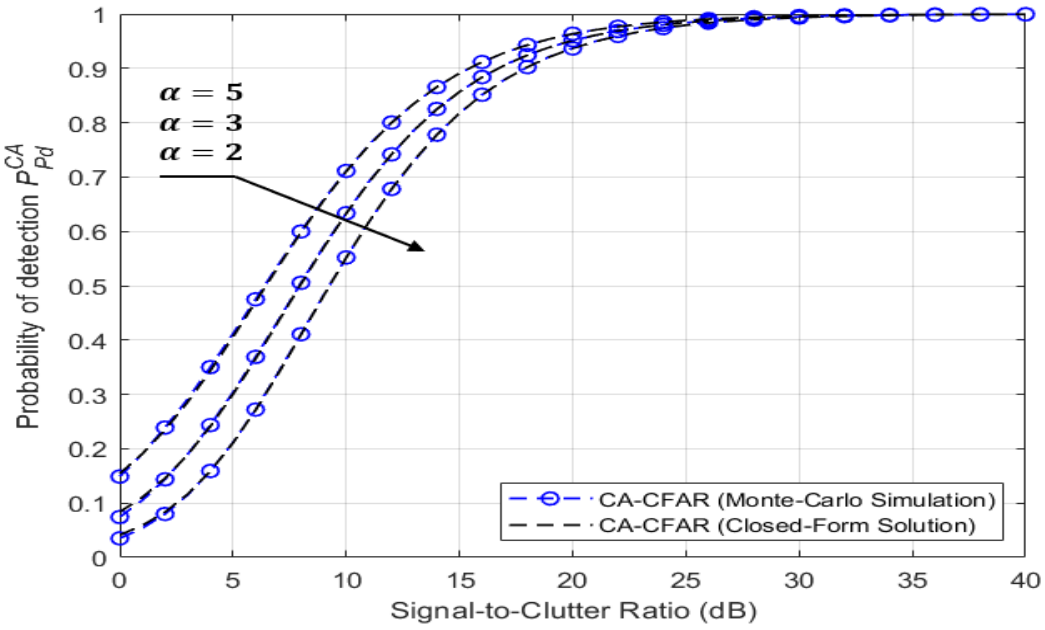

Figure III.15: Probability of detection of CA-CFAR against the SCR for **N=12** $\boldsymbol{\beta}$ = **1**, $\boldsymbol{P_{fa} = 10^{-4}}$ and different values of $\boldsymbol{\alpha}(\boldsymbol{\alpha = 2, 3}\ \textit{and}\ \boldsymbol{5})$

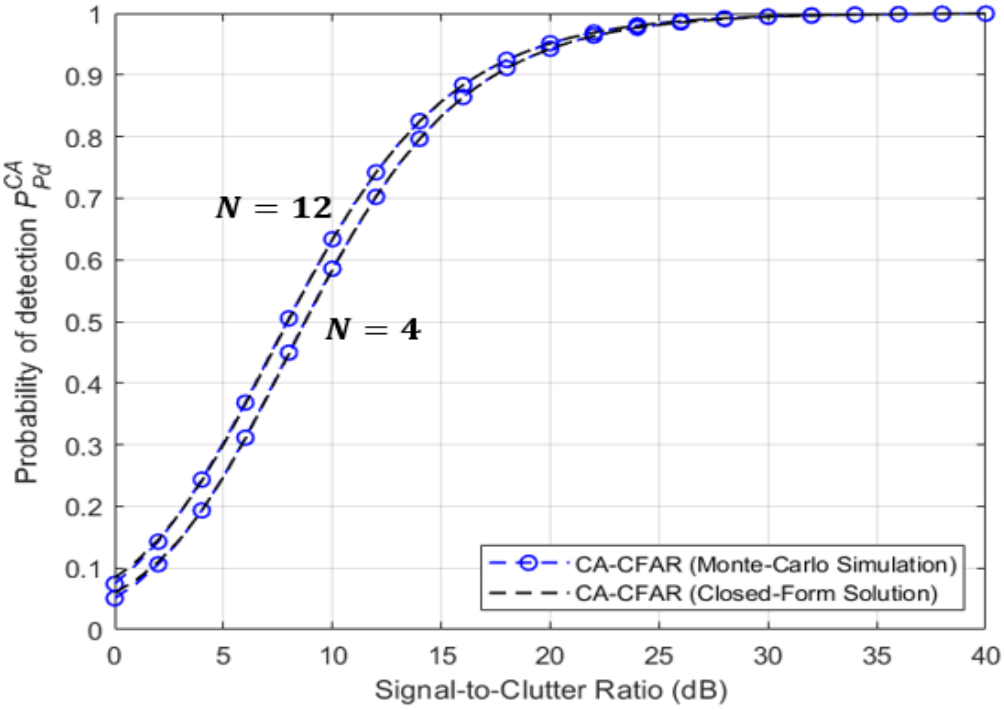

Figure III.16: Probability of detection of CA-CFAR against the SCR for $\boldsymbol{\alpha}$=**3** $\boldsymbol{\beta}$ = **1,** $\boldsymbol{P_{fa} = 10^{-4}}$ and different values of $\boldsymbol{N}$($\boldsymbol{N = 4}$ *and* **12**)

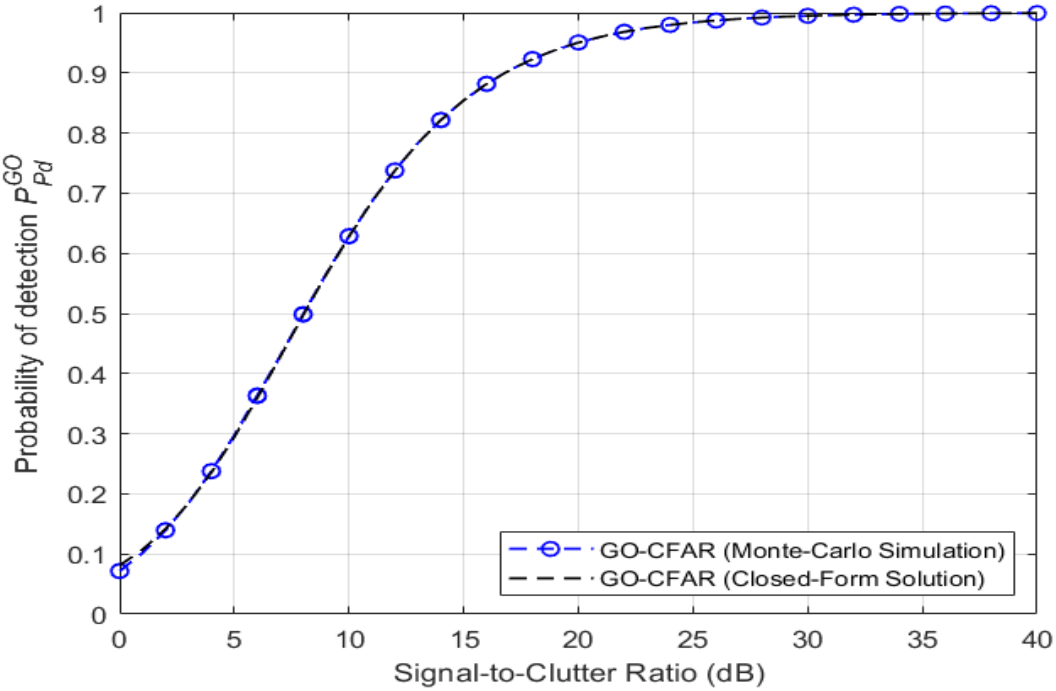

Figure III.17: Probability of detection the GO-CFAR detector against the SCR for $\boldsymbol{\alpha = 3}$

N= 12, $\boldsymbol{P_{fa} = 10^{-4}}$ different values of $\boldsymbol{\beta}$($\boldsymbol{\beta}$ = **1,5** and **50**)

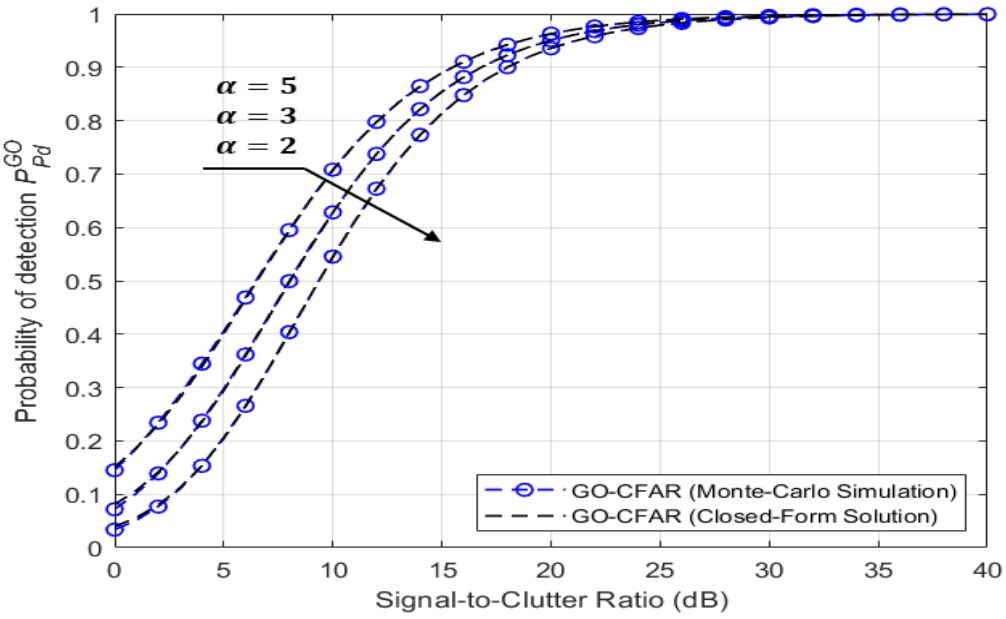

Figure III.18: Probability of detection of GO-CFAR against the SCR for **N=12** $\boldsymbol{\beta = 1, P_{fa} = 10^{-4}}$ and different values of $\boldsymbol{\alpha(\alpha = 2, 3\ and\ 5)}$

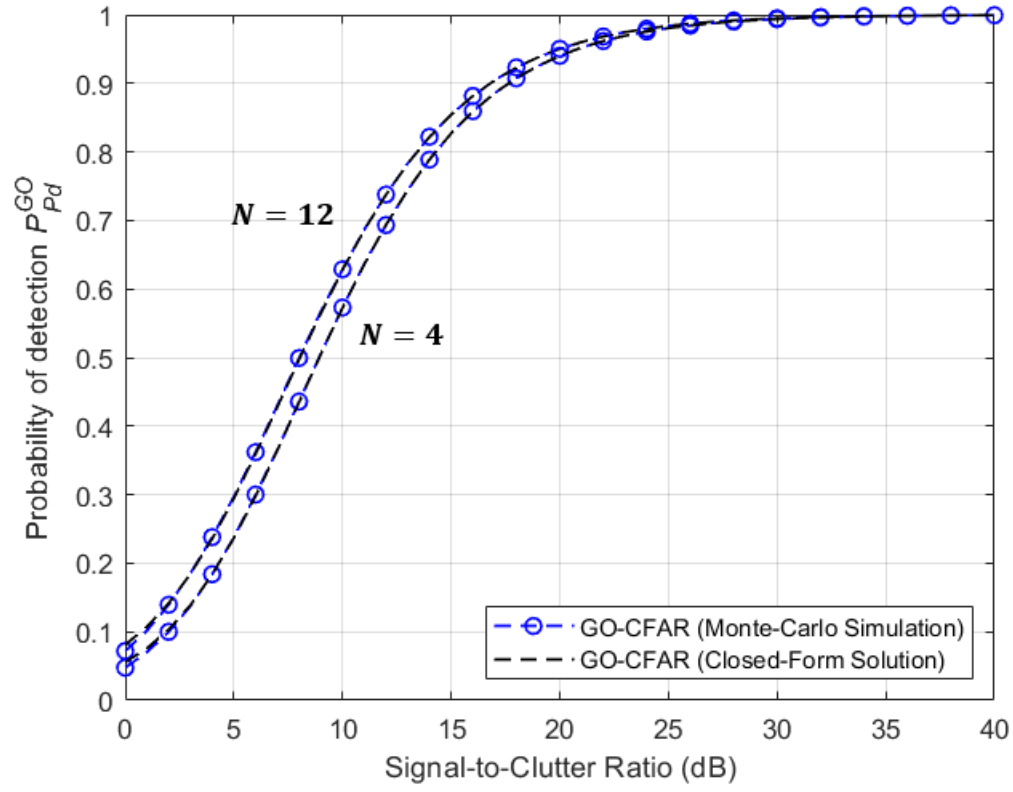

Figure III.19: Probability of detection of GO-CFAR against the SCR for $\boldsymbol{\alpha}$**=3** $\boldsymbol{\beta = 1, P_{fa} = 10^{-4}}$ and different values of $\boldsymbol{N(N = 4\ and\ 12)}$

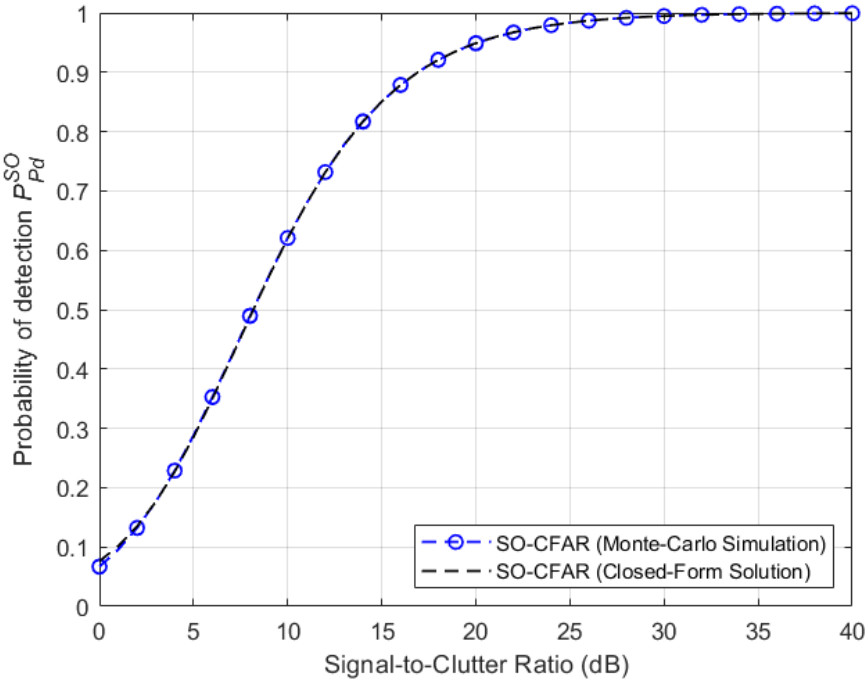

Figure III.20: Probability of detection the SO-CFAR detector against the SCR for $\boldsymbol{\alpha = 3}$ **N= 12**, $\boldsymbol{P_{fa} = 10^{-4}}$ different values of $\boldsymbol{\beta}$($\boldsymbol{\beta}$ = **1**,**5** and **50**)

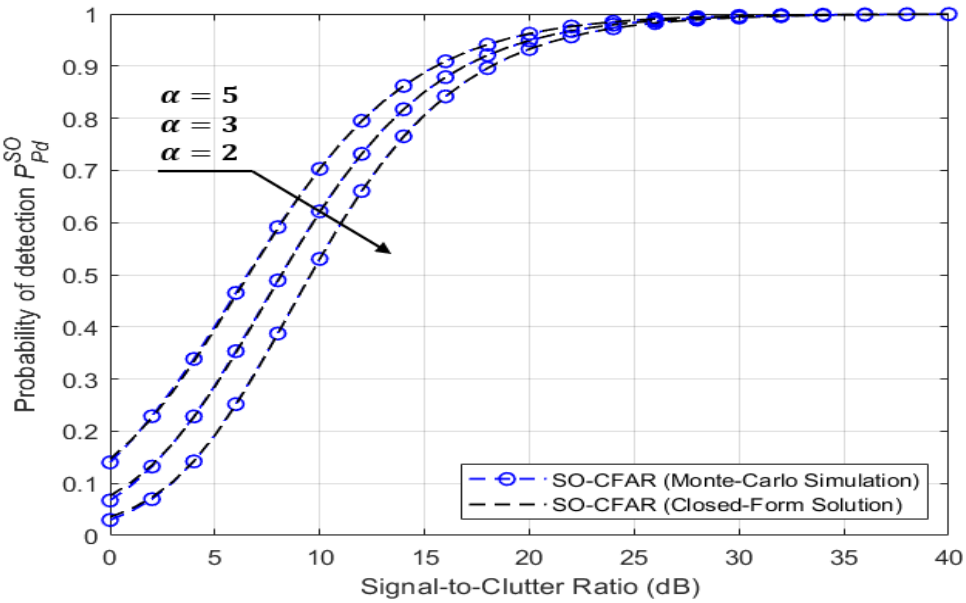

Figure III.21: Probability of detection of SO-CFAR against the SCR for **N=12** $\boldsymbol{\beta = 1, P_{fa} = 10^{-4}}$ and different values of $\boldsymbol{\alpha(\alpha = 2, 3\ and\ 5)}$

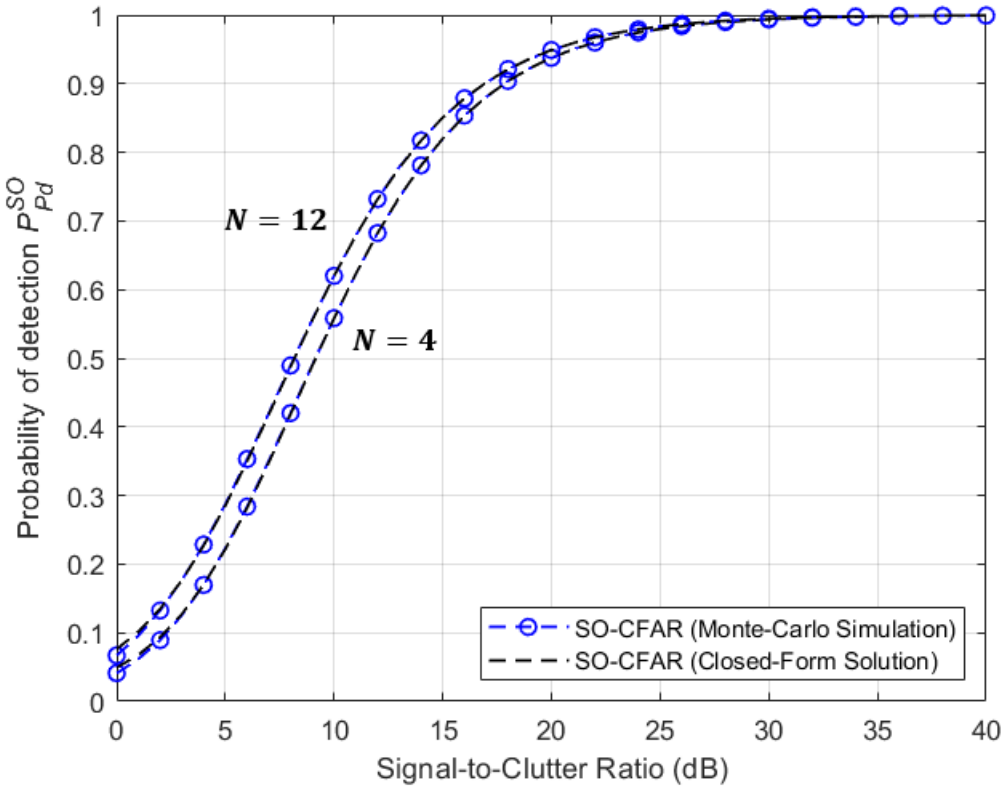

Figure III.22: Probability of detection of SO-CFAR against the SCR for $\boldsymbol{\alpha}$=3 $\boldsymbol{\beta} = 1, \boldsymbol{P_{fa}} = \boldsymbol{10^{-4}}$ and different values of $\boldsymbol{N}(\boldsymbol{N} = 4 \; and \; 12)$

III.4 Comparison of detection performance of Optimal, CA, GO and SO

III.4.1 Case of homogeneous clutter

In this section, we compare the detection performance of the Optimal, CA-, GO- and SO-CFAR processors under the assumption of homogeneous Gamma-distributed clutter. Multiple performance scenarios are examined by varying key simulation parameters, namely the shape parameter α, the scale parameter N, and the desired probability of false alarm P_{fa}. For benchmarking purposes, the optimal detector is also included in the analysis. The resulting performance comparisons are illustrated in Figures III.23, III.24, and III.25.

Figure III.23 illustrates the impact of the Gamma clutter shape parameter α on the detection performance of several CFAR detectors. The probability of detection (P_d) is plotted against the signal-to-clutter ratio (SCR) in dB, under two clutter conditions: $\alpha = 2$ and $\alpha = 5$. These values

represent different degrees of homogeneity in the clutter; lower α indicates more impulsive or heterogeneous clutter, while higher α reflects more homogeneous conditions.

The figure includes performance curves for the Optimal detector and three practical CFAR schemes: CA-CFAR, GO-CFAR, and SO-CFAR. Two zoomed-in insets are presented to emphasize performance variations in the mid-SCR region for both α\alphaα cases.

Clutter with $\alpha = 2$

In the impulsive clutter scenario ($\alpha = 2$), all CFAR detectors show degraded performance compared to the Optimal detector, particularly in the SCR range of 5–15 dB. The performance gap is most noticeable for the SO-CFAR, which exhibits the lowest P_d values among the practical schemes. The CA-CFAR and GO-CFAR detectors perform comparably in this regime, with CA-CFAR slightly outperforming GO -CFAR due to its design resilience against interfering targets.

Clutter with $\alpha = 5$

For $\alpha = 5$, the clutter becomes more homogeneous, and all detectors demonstrate significantly improved detection performance. The gap between practical CFAR schemes and the Optimal detector is reduced, particularly in the transition region where P_d rapidly increases with SCR. Notably, both CA-CFAR and GO-CFAR converge more closely to the Optimal detector's performance, indicating their increased effectiveness in well-behaved clutter environments. The SO-CFAR continues to lag slightly behind, consistent with its conservative thresholding strategy

Figure III.24 presents a comparative analysis of the detection performance of various CFAR algorithms as a function of the number of reference cells N. The probability of detection (P_d) is plotted against the signal-to-clutter ratio (SCR) in decibels for two distinct values of N: N=4 and N=12. The evaluated detection schemes include the CA-CFAR, GO-CFAR, SO-CFAR, and the Optimal detector, the latter serving as the performance benchmark.

Effect of Reference Window Size

The results clearly show that increasing the number of reference cells significantly enhances the detection performance of practical CFAR detectors. This improvement is particularly evident in the mid-SCR range (approximately 5–15 dB), as highlighted by the zoomed-in insets in the figure.

- For N=4, the performance gap between practical CFAR schemes and the Optimal detector is more pronounced. The limited number of reference cells leads to less accurate estimation of background clutter power, resulting in suboptimal threshold setting and degraded P_d, especially for the SO-CFAR detector.
- For N=12, all CFAR detectors show substantial performance gains, with detection curves moving closer to the Optimal detector's performance. The increased sample size allows for more reliable estimation of clutter statistics, thereby enhancing threshold accuracy and improving detection probability.

Detector Comparisons

Across both values of N, the CA-CFAR generally outperforms the GO-CFAR and SO-CFAR, particularly in the SCR range of interest. This superiority stems from its design, which uses ordered statistics to mitigate the effect of interfering targets. The SO-CFAR performs worst among the three in homogeneous environments, as it is more conservative in adapting its threshold to potential outliers, which are absent in the current scenario.

The graph in Figure III.25 illustrates the probability of detection P_d as a function of the signal-to-clutter ratio (SCR) for various CFAR (Constant False Alarm Rate) algorithms, including CA-CFAR, GO-CFAR, SO-CFAR, and an optimal detector. The analysis is conducted for two different false alarm probabilities: $P_{fa} = 10^{-4}$ and $P_{fa} = 10^{-4}$.

As expected, all detectors exhibit an increasing $P_d$with rising SCR.

At both false alarm levels:

CA-CFAR provides better robustness than GO -CFAR, particularly in clutter edges or when strong targets are nearby, as it ignores high-power cells.

CA-CFAR shows improved detection in multi-target scenarios by rejecting both the smallest and greatest values in the reference cells, providing a more balanced estimation.

SO-CFAR tends to underperform in homogeneous environments due to its sensitivity to interfering targets within the reference window.

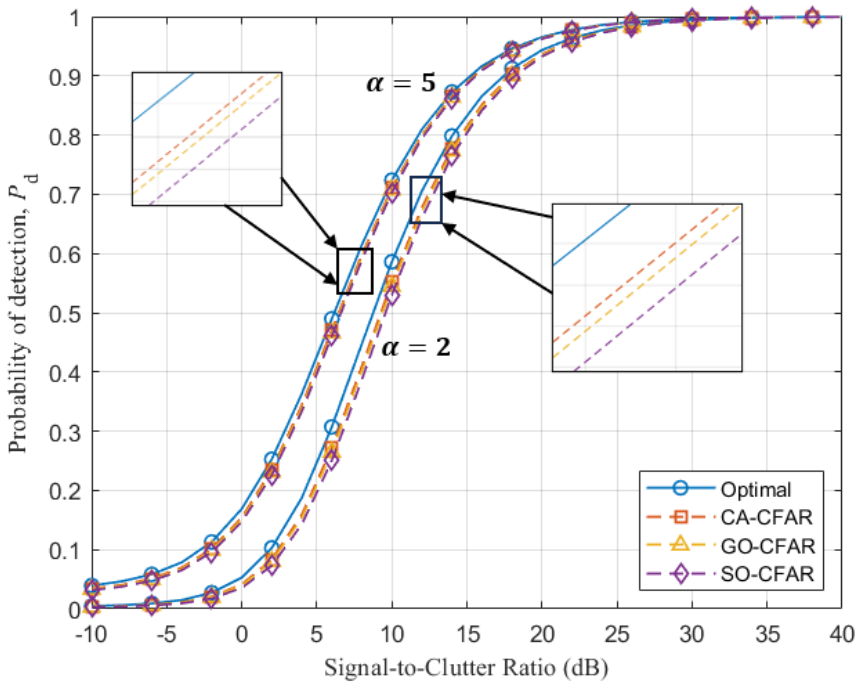

Figure III.23: Comparison of detection performance of Optimal, CA, GO-and SO-CFAR detector for $\boldsymbol{\beta = 1, P_{fa} = 10^{-4}}$ N=12 and different values of $\boldsymbol{\alpha(\alpha = 2\ and\ 5)}$

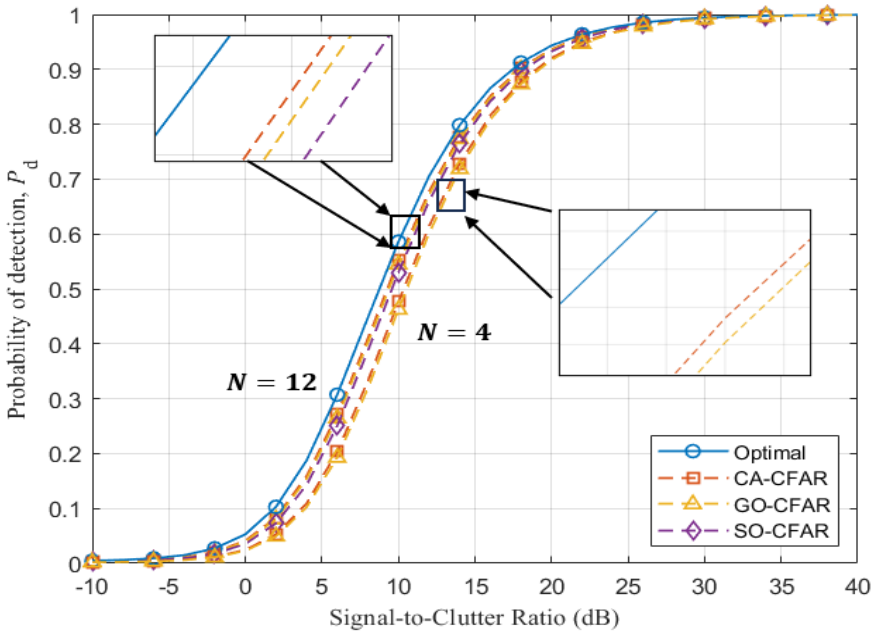

Figure III.24: Comparison of detection performance of Optimal, CA, GO-and SO-CFAR detector for $\boldsymbol{\beta = 1\ \ P_{fa} = 10^{-4}\ \alpha}$ =2 and different values of $\boldsymbol{N(N = 4\ and\ 12)}$

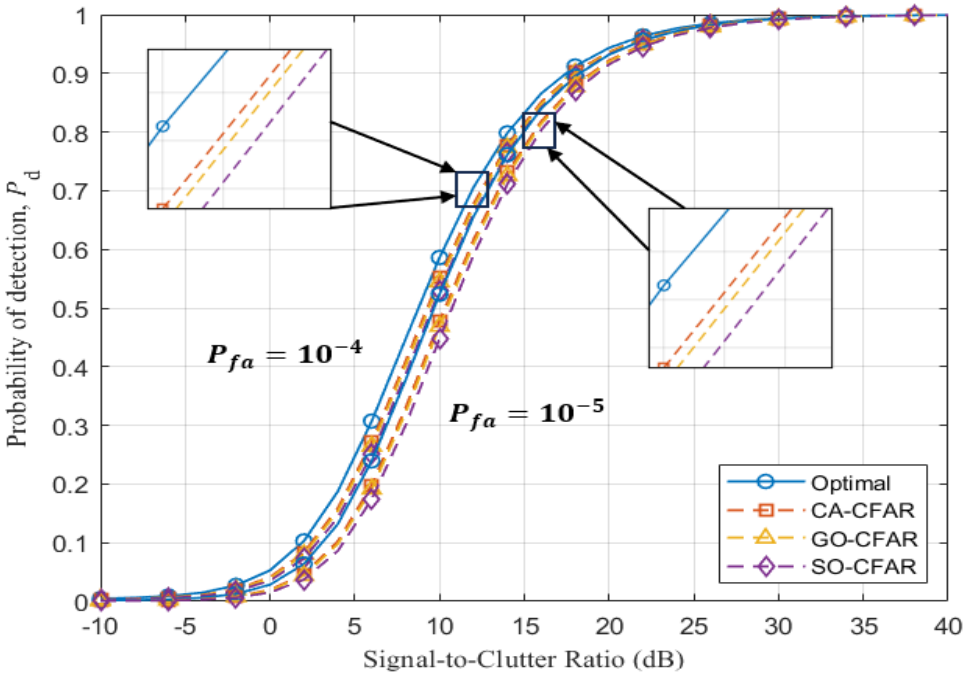

Figure III.25: Comparison of detection performance of Optimal, CA, GO-and SO-CFAR detector for $\boldsymbol{\beta} = \mathbf{1}, \boldsymbol{N} = \mathbf{12}$ $\boldsymbol{\alpha}$ =2 and different values of $\boldsymbol{P_{fa}}(\boldsymbol{P_{fa}} = \mathbf{10^{-4}}\ and\ \mathbf{10^{-5}})$

III.4.2 Case of non homogeneous clutter

In this section, we compare the detection performance of the Optimal, CA-, GO-, and SO-CFAR processors under the assumption of Non-homogeneous Gamma-distributed clutter .Multiple performance scenarios are examined by interfering target in window . With stabilizing the shape parameter α, the scale parameter N, and the desired probability of false alarm P_{fa} constantThe resulting performance comparisons are illustrated in Figures III.26, III.27, and III.28.

Figure III.26 presents a comparative analysis of the detection performance of four CFAR detection schemes Optimal, CA-CFAR, GO-CFAR, and SO-CFAR in the presence of one interfering target. The evaluation is conducted under the following parameters: Interference-to-Clutter Ratio (ICR) = 20 dB, shape parameter α=2, scale parameter β=1, false alarm probability $P_{fa} = 10^{-4}$, and number of reference cells N=12.

As expected, the optimal detector achieves the best performance, providing the highest probability of detection P_d across all Signal-to-Clutter Ratios (SCR). This curve serves as the benchmark for comparing the performance of CFAR-based detectors.

The SO-CFAR shows better detection performance than both CA-CFAR and GO-CFAR in low and medium SCR regions, particularly under the presence of an interfering target. This is consistent with its design, as SO-CFAR is more resistant to outliers and interference due to its reliance on the minimum of two local estimates for noise power.

CA-CFAR demonstrates improved performance over GO-CFAR, especially in the presence of interference. While CA-CFAR assumes homogeneity, its performance deteriorates significantly in non-homogeneous or interfered backgrounds. GO-CFAR mitigates this effect by using the maximum of the two estimates, which protects against masking effects.

Figure III.27 illustrates the detection performance comparison among four detection schemes Optimal, CA-CFAR, GO-CFAR, and SO-CFAR—in the presence of two interfering targets located within the same sliding window (Semu-window). The simulation is conducted under the following parameters: Interference-to-Clutter Ratio (ICR) = 20 dB, shape parameter α=2, scale parameter β=1, false alarm probability $P_{fa} = 10^{-4}$, and number of reference cells N=12.

Among the three CFAR detectors, SO-CFAR demonstrates the best performance, closely approximating the Optimal detector's behavior across all SCR values. This confirms its robustness in the presence of multiple interferences, as it relies on the minimum of the leading and lagging window statistics, thereby reducing the impact of interference contamination.

CA-CFAR, while designed to mitigate target masking in heterogeneous environments, shows poorer performance in this specific configuration. Its reliance on the maximum of the reference windows causes it to be overly conservative, leading to reduced detection probability, especially at lower SCR levels.

GO-CFAR exhibits the worst detection performance in the presence of two interferers. Since it averages all training cells, the presence of strong interfering signals inflates the estimated noise power, leading to excessively high thresholds and hence lower detection probabilities.

Figure III.28 compares the detection performance of the Optimal, CA-CFAR, GO-CFAR, and SO-CFAR detectors under an asymmetrical interference scenario. In this case, one interfering target is present in the leading window with an Interference-to-Clutter Ratio (ICR) of 20 dB, and another interfering target is present in the lagging window with an ICR of 10 dB. The other parameters:

shape parameter α=2, scale parameter β=1, false alarm probability $P_{fa} = 10^{-4}$, and number of reference cells N=12.

Impact of Asymmetrical Interference:

The interference is no longer uniformly distributed between the reference windows, which introduces asymmetry into the background noise estimation. This setup tests each detector's robustness to uneven contamination.

As with previous scenarios, SO-CFAR maintains relatively strong performance. Its reliance on the minimum of the two window estimates makes it especially effective here, as it tends to ignore the more heavily contaminated estimate. It performs significantly better than CA- and GO-CFAR and approaches the Optimal detector in high SCR regions.

CA-CFAR is particularly vulnerable in this configuration. Since it uses the maximum of the two window estimates, it often overestimates the noise level due to the high interference in the leading window (ICR = 20 dB). As a result, its threshold is set too high, leading to poor detection probability at low and moderate SCR values.

The GO-CFAR detector, performs better than CA-CFAR but worse than SO-CFAR. Its performance is degraded due to averaging over both contaminated windows, which still raises the threshold beyond optimal levels.

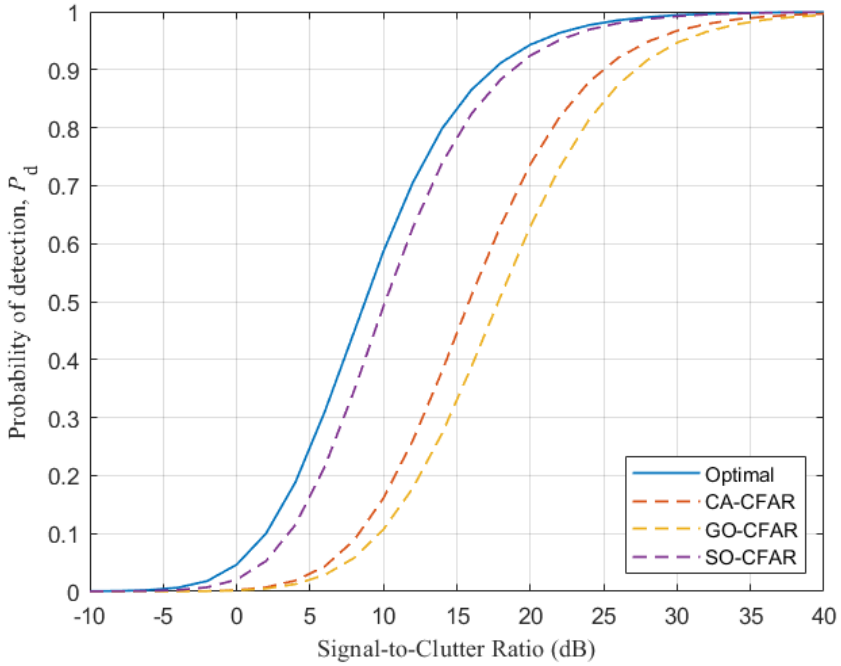

Figure III.26: Comparison of detection performance of Optimal, CA, GO-and SO-CFAR detector for one interfering target **ICR=20dB,** $\boldsymbol{\beta = 1, P_{fa} = 10^{-4}}$ **,N=12** and of $\boldsymbol{\alpha = 2}$

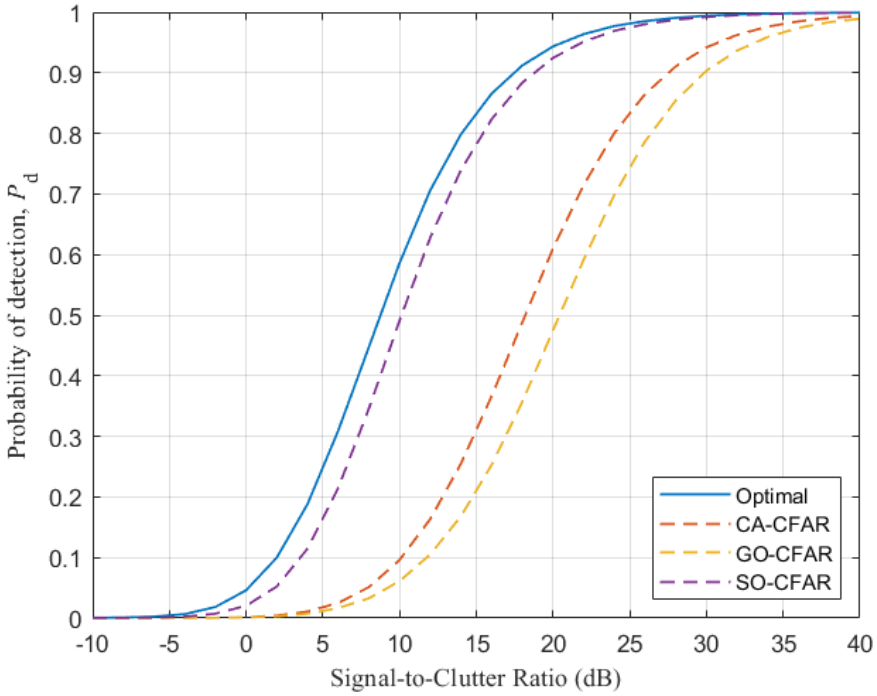

Figure III.27: Comparison of detection performance of Optimal, CA, GO-and SO-CFAR detector for two interfering target in the same Semu-window **ICR=20dB,** $\boldsymbol{\beta = 1, P_{fa} = 10^{-4}}$, **N=12** and of $\boldsymbol{\alpha = 2}$

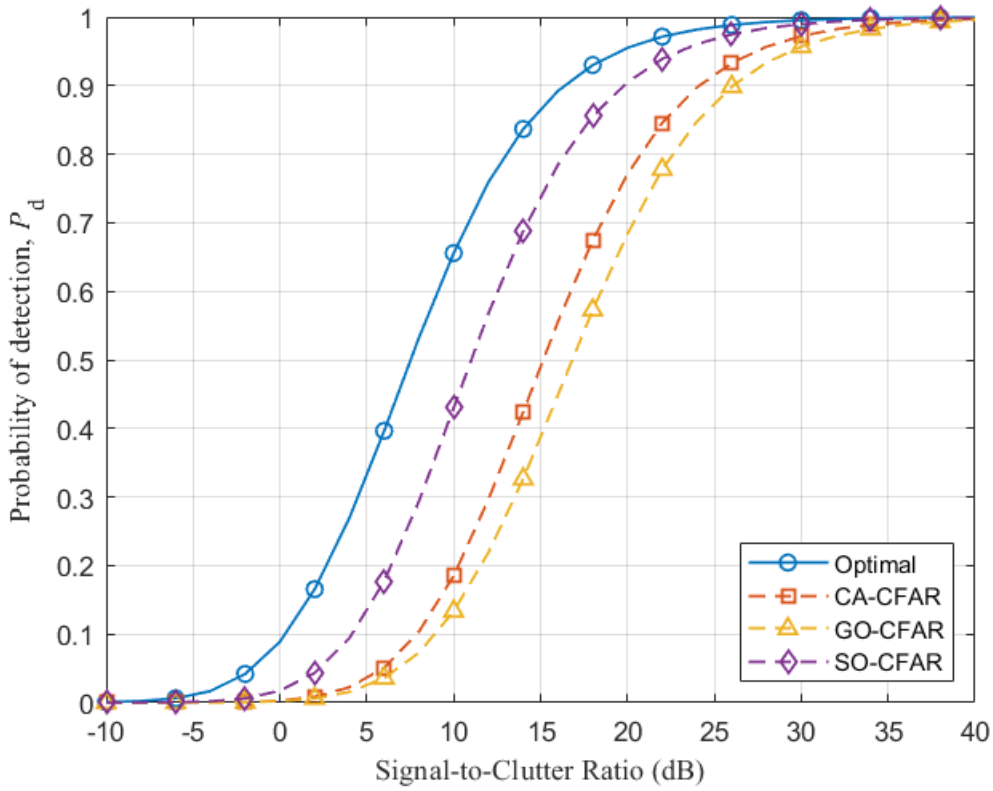

Figure III.28: Comparison of detection performance of Optimal, CA, GO-and SO-CFAR detector for one interfering target in the Leading-window **ICR=20dB** and one interfering target in the Logging-window **ICR=10dB,** $\boldsymbol{\beta = 1}$, $\boldsymbol{P_{fa} = 10^{-4}}$, **N=12** and of $\boldsymbol{\alpha = 2}$

III.5. Conclusion

This chapter presents a numerical validation of the closed-form expressions for the false alarm probability and the proposed approximations of the detection probability for the CA-, GO-, and SO-CFAR detectors. The results demonstrate a high degree of agreement between the derived expressions and those obtained via numerical integration and Monte Carlo simulations. Subsequently, the detection performance of the Optimal, CA-, GO-, and SO-CFAR algorithms was evaluated under both homogeneous and non-homogeneous clutter conditions. The analysis was conducted by varying the shape parameter of the Gamma distribution, the size of the reference window, and the target false alarm probability. The results indicate that the SO-CFAR detector exhibits robust performance in non-homogeneous environments characterized by Gamma-distributed clutter, thereby validating its suitability in such scenarios

Conclusion and Perspectives

General Conclusion

In this master's dissertation, we addressed the problem of Constant False Alarm Rate (CFAR) target detection in both homogeneous and non-homogeneous clutter modeled by a Gamma distribution. This problem is of significant relevance in radar systems and remote sensing applications.

The study focused on the performance analysis of three mean-level CFAR detectors: Cell Averaging (CA), Greatest Of (GO), and Smallest Of (SO). A comprehensive theoretical analysis was conducted for each algorithm. The first contribution of this work lies in the derivation of two closed-form expressions for the false alarm probability P_{fa} applicable to all detectors.

Furthermore, it was observed that the exact computation of the detection probability P_d, based on the precise statistical distribution of the cell under test, involves complex integrals that are difficult to evaluate numerically. To address this challenge, an approximation of the test cell statistics was introduced, yielding two novel, tractable expressions for the detection probability. These approximations are more amenable to numerical evaluation and suitable for implementation in real-time systems.

The proposed expressions for P_{fa} and P_d were subsequently validated through numerical simulations and compared against results obtained using numerical integration methods and Monte Carlo simulations. Additionally, the detection performance of the CA, GO, and SO CFAR detectors was analyzed and compared to that of the optimal detector. The results indicate that the SO-CFAR detector achieves satisfactory performance in homogeneous clutter environments relative to CA and GO-CFAR detectors but exhibits some CFAR loss when compared to the optimal detector.

References

[1] M. Skolnik, Introduction to Radar System, (3rd ed.), New York: McGraw-Hill, 2001.

[2] M. Sahed, *Radar Systems, Course material,* M'Sila: University of M'Sila, 2020.

[3] R. Buderi, The Invention that Changed the World, Touchstone edition, 1998.

[4] E. Jakeman and P. N. Pusey, "A model of non-Rayleigh Sea echo," *IEEE Transactions on Antennas and Propagation,* vol. 24, no. 6, pp. 806-914, 1976.

[5] E. Jakeman and P. Pusey, "Significance of K distributions in scattering experiments," vol. 40, no.

9, p. 546–550, Feb. 1978..

[6] D. K. Ward, "Compound representation of high-resolution sea clutter," *Electronics Letters,* vol.17, no. 16, pp. 561-563, 1981.

[7] M. Sahed, E. Kenane, A. Khalfa and F. Djahli, "Exact Closed-Form Pfa Expressions for CA- and GO-CFAR Detectors in Gamma-Distributed Radar Clutter," *IEEE Trans. Aerosp. Electron. Syst,*vol. Doi: 10.1109/TAES.2022.3232101., 2023.

[8] F. D. A. García, A. C. F. Rodriguez, G. Fraidenraich and J. C. S. S. Filho, "CA-CFAR Detection Performance in Homogeneous Weibull Clutter," *Remote. Sens. Lett,* vol. 16, no. 4, p. 887–891, Jun. 2019.

[9] C. Schleher, "Radar detection in Weibull clutter," *IEEE Transactions on Aerospace and Electronic Systems,* vol. 12, no. 6, pp. 736-743, 1976.

[10] M. Guida, M. Longo and M. Lops, "Biparametric CFAR procedures for lognormal clutter," *Aerosp. Electron. Syst,* vol. 29, no. 3, p. 798–809, Jul. 1993.

[11] W. Zhou, J. Xie, G. Li and Y. Du, "Robust CFAR detector with weighted amplitude iteration in nonhomogeneous sea clutter," *Aerosp. Electron. Syst,* vol. 53, no. 3, p. 1520–1535, Jun. 2017.

[12] S. Kay, Fundamental Of Statistical Signal Processing: Detection Theory, Englwood Cliffs: Prentice Hall, 1998.

[13] M. Sahed, "Détection Automatique CFAR en environnement Non Gaussien,"," Thèse de Doctorat ès science, Université de M'sila, 2015.

[14] P. A, "On adaptive censored CFAR detection," Thèse de Doctorat, New Jersey Institute of

Technology, 1993.

[15] P. Gandhi and S. A. Kassam, "Optimality of the cell averaging CFAR detector," IEEE Transactions on Information Theory, vol. 40, no. 4, pp. 1226-1228, 1994.

[16] P. P. Gandhi and S. A. Kassam, "Analysis of CFAR processors in nonhomogeneous background," IEEE Transactions on Aerospace and Electronic Systems, vol. 24, no. 4, pp. 427-445, 1988.

[17] S. Watts, "Cell-averaging CFAR gain in spatially correlated K-distributed clutter," Radar, Sonar and Navigation, vol. 143, no. 5, p. 321–327, Oct. 1996..

[18] G. Minkler and J. Minkler, CFAR – the principles of automatic radar detection in clutter,

Baltimore: Magellan, 1990.

[19] M. Sahed, "Détection CFAR dans un clutter de mer de distribution K avec des paramètres

inconnus en présence du bruit thermique," Mémoire de Magistère, Université de M'sila, Algérie.,

2010.

[20] S. George, The detection of nonfluctuating targets in log-normal clutter, Washington, DC, USA,: Naval Research Laboratory., Oct. 1968..

[21] K. Krishnamoorthy, Handbook of Statistical Distributions with Applications,", USA: Chapman & Hall/CRC, 2006.

[22] F. Gini, F. Lombardini and L. Verrazzani, "Decentralized CFAR detection with binary integration in Weibull clutter," IEEE Trans. Aerosp. Electron. Syst., vol. 33, no. 2, pp. 396-407, Apr. 1997.

[23] R. Ravid and N. Levanon, "Maximum-likelihood CFAR for Weibull background," IEE

Proceedings, Radar, Sonar and Navig., vol. 139, no. 3, pp. 256-264, Jun. 1992..

[24] M. Abramowitz and I. A. Stegun, Handbook of Mathematical Functions, New York: Dover

Publications, Inc., 1970.

[25] I. S. Gradshteyn and I. M. Ryzhik, Table of Integrals, Series, and Products, San Diego: Academic Press, 2015.

[26] H. M. F. a. R. S. A. Johnson, "Adaptive detection model with threshold control as function of

spatially sampled clutter-level estimates," RCA Rev, vol. 29, p. 414–464, 1968.

[27] S. B. Opps, N. Saad and H. M. Srivastava, "Some reduction and transformation formulas for the Appell hypergeometric function F2," J. Math. Anal. Appl, Vols. 302,, no. 1, pp. 180-195, Feb.

2005..

Abstract:

This study investigates the problem of adaptive radar target detection in both homogeneous and non-homogeneous Gamma-distributed clutter environments. The objective is to maintain a Constant False Alarm Rate (CFAR) during the detection process. It is assumed that the radar system employs a square-law detector preceding the CFAR processing stage.

Initially, the fundamental principles of radar target detection in noise are presented, along with an overview of CFAR detection techniques. The study then focuses on a detailed examination of several Mean-Level CFAR detectors operating in Gamma-distributed clutter, specifically the Cell Averaging (CA-CFAR), Greatest Of (GO-CFAR), and Smallest Of (SO-CFAR) algorithms.

A comprehensive theoretical analysis is conducted for each detector. Closed-form expressions for the probability of false alarm (Pfa) are derived. However, the calculation of the probability of detection (Pd), based on the exact statistical characterization of the cell under test (CUT), involves complex integrals that are computationally intensive. To address this issue, approximate expressions for Pd are proposed. These approximations offer computational efficiency and are suitable for real-time implementation.

The theoretical findings are validated through numerical evaluation, including both integral-based computations and Monte Carlo simulations, under various clutter scenarios. Furthermore, a performance comparison between the studied detectors and the optimal detector is performed, assuming a homogeneous clutter environment.

The results demonstrate that the SO-CFAR detector exhibits superior performance in homogeneous clutter, while the GO-CFAR detector proves to be more effective in non-homogeneous environments.

ملخص:

تبحث هذه الدراسة في مشكلة الكشف التكيفي عن أهداف الرادار في بيئات فوضى متجانسة وغير متجانسة موزعة بأشعة غاما. الهدف هو الحفاظ على معدل ثابت للإنذارات الكاذبة (CFAR) أثناء عملية الكشف. يُفترض أن نظام الرادار يستخدم كاشف قانون التربيع قبل مرحلة معالجة CFAR.

في البداية، تُعرض المبادئ الأساسية للكشف عن أهداف الرادار في الضوضاء، بالإضافة إلى لمحة عامة عن تقنيات الكشف عن CFAR. ثم تُركز الدراسة على فحص مُفصل للعديد من كاشفات CFAR متوسطة المستوى العاملة في فوضى موزعة بأشعة غاما، وتحديدًا خوارزميات متوسط الخلايا (CA-CFAR)، وأكبر قيمة (GO-CFAR)، وأصغر قيمة (SO-CFAR).

يُجرى تحليل نظري شامل لكل كاشف. وتُشتق تعابير مغلقة الشكل لاحتمالية الإنذارات الكاذبة (Pfa). ومع ذلك، فإن حساب احتمال الكشف (Pd)، بناءً على التوصيف الإحصائي الدقيق للخلية قيد الاختبار (CUT)، يتضمن تكاملات معقدة تتطلب حسابات مكثفة. ولمعالجة هذه المشكلة، تُقترح تعابير تقريبية لـ Pd. توفر هذه التقريبات كفاءة حسابية وهي مناسبة للتطبيق الفوري.

تم التحقق من صحة النتائج النظرية من خلال التقييم العددي، بما في ذلك الحسابات التكاملية ومحاكاة مونت كارلو، في ظل سيناريوهات فوضى متنوعة. علاوة على ذلك، أُجريت مقارنة بين أداء الكواشف المدروسة والكاشف الأمثل، بافتراض بيئة فوضى متجانسة.

أظهرت النتائج أن كاشف SO-CFAR يُظهر أداءً متفوقًا في بيئة فوضى متجانسة، بينما أثبت كاشف GO-CFAR أنه أكثر فعالية في البيئات غير المتجانسة.